

Compile-once block encodings for masked similarity-transformed effective Hamiltonians

Bo Peng,^{1,*} Yuan Liu,² and Karol Kowalski¹

¹*Physical and Computational Sciences Directorate,
Pacific Northwest National Laboratory, Richland, Washington 99354, United States*

²*Department of Electrical and Computer Engineering,
Department of Computer Science, Department of Physics,
North Carolina State University, Raleigh, North Carolina 27695, USA*

(Dated: March 3, 2026)

We present **COMPOSER**, a compile-once modular parametric oracle for similarity-encoded effective reduction of electronic-structure operators (e.g., Schrieffer–Wolff-type constructions). Low-rank factorizations compress Hamiltonians and anti-Hermitian generators into rank-one bilinear and projected-quadratic ladders with near-linear scaling at fixed thresholds; each ladder admits deterministic, number-conserving preparation and a block encoding using constant number of signal ancillas. A fixed **PREP–SELECT–PREP**[†] template multiplexes these ladders, and one QSP polynomial performs the spectral transformation with degree set by operator norms. For a fixed orbital pool and qubit register, the two-qubit fabric is compiled once; geometry, active-space (mask) updates, and truncations are absorbed by re-dialed single-qubit rotations. We introduce a mask-aware similarity-sandwich effective-Hamiltonian construction and benchmark stability under low-rank and second-order-perturbation-guided screening. **COMPOSER** is an execution architecture: algorithmic errors (block-encoding and QSP approximation) are tunable for any supplied parameters, while physical accuracy depends on how those parameters are obtained if not refined.

CONTENTS

I. Introduction	2	V. Architecture, and Compile–Once Philosophy of COMPOSER	15
II. Rank-One Representations of Quantum-Chemistry Operators	5	VI. Relation to Local Jastrow Ansatz, Tensor Networks, and Canonical Transformations	17
A. Rank-one operators	5	VII. Numerical Demonstration	18
B. Rank-one representation of the molecular Hamiltonian	6	VIII. Conclusion and Outlook	21
C. Rank-one representation of the cluster generator	7	Acknowledgments	21
III. Deterministic preparation of one- and two-electron states	8	A. Deterministic Ladder Constructions and Hardware Realizations	22
A. Deterministic preparation of the one-electron state	8	1. One-electron ladder: recursion and explicit product form	22
B. Deterministic preparation of a two-electron state	9	2. Two-electron ladder: recursion and explicit product form	22
IV. Block encoding of rank-one operators	10	3. Two-Electron Givens–SWAP Networks and Hardware Mapping	22
A. Encoding rank-one operators	10	4. Preparation versus number-conserving ladder forms	23
B. Encoding exponentials of rank-one generators	11	B. Proofs and implementation details for rank-one block encodings	23
C. Similarity–sandwiched effective Hamiltonian	12	1. Proof of Lemma 1	23
D. Resource analysis and practical advantages	14	2. Proof of Lemma 2	25
		3. Proof of Theorem 1	25
		C. Quantum Signal Processing for Exponentiating Block-Encoded Generators	26

* peng398@pnnl.gov

1. Polynomial approximation	26
2. QSP implementation	26
3. Error propagation	26
4. Application to the generator $\hat{\sigma}$	27
D. Compile–Once Architecture and Error–Depth Tradeoffs	27
1. Selector-controlled adaptor overhead	27
2. Depth scaling versus error tolerance	27
3. Error-budget allocation	27
4. Meaning of “compile–once”	28
E. Diagnostics for Fixed Rank–One Algebraic Formulations	28
1. Subspace stability diagnostics	28
2. Subspace-overlap metric for rank-one manifolds (wAUC)	29
3. MP2-guided construction of truncated rank–one operator lists	29
References	30

I. INTRODUCTION

Quantum computation promises to transform how we model and understand many-body quantum systems, particularly in regimes where classical approaches encounter exponential scaling bottlenecks. In quantum chemistry and materials science, core tasks such as computing ground- and excited-state energies, simulating real-time dynamics, and extracting mechanistic insight from correlated electronic structure remain computationally demanding even on the most advanced classical platforms [1–11]. Beyond static ground-state properties, there is growing interest in quantum algorithms for dynamics, spectroscopy, transport, and temperature-dependent phenomena, which place additional demands on both algorithmic design and circuit-level efficiency [12–17]. Beyond phase-estimation-based approaches, NISQ-era methods such as quantum imaginary-time evolution and Krylov/Lanczos-type procedures provide alternatives for ground- and excited-state estimation [18, 19].

As fault-tolerant quantum computing (FTQC) architectures begin to take shape, attention has increasingly shifted from asymptotic algorithmic scaling alone toward the full execution stack required for scientifically relevant workloads. This includes state preparation, operator encoding, time evolution, and observable estimation, as well as the classical–quantum feedback loops that arise in adaptive and iterative workflows [17, 20–27]. In this setting, circuit compilation, data loading, and reuse

across closely related problem instances can dominate wall-clock cost and strongly influence practical feasibility. A central tension therefore emerges: electronic-structure operators possess rich algebraic structure, such as low-rank factorizations, excitation hierarchies, and subspace locality, while quantum circuit implementations typically flatten these structures into instance-specific gate sequences. As a result, closely related problem instances often trigger structural recompilation of multiplexing trees and routing layers, even when the underlying operator algebra changes only parametrically. A second, closely related source of recompilation overhead arises in *subspace diagonalization* and *subspace expansion* algorithms. In this family of methods one constructs an effective Hamiltonian and overlap matrix, $H_{ij} = \langle \psi_i | \hat{H} | \psi_j \rangle$ and $S_{ij} = \langle \psi_i | \psi_j \rangle$, in a (generally non-orthogonal) basis of parametrized states $\{|\psi_i\rangle\}_{i=1}^K$ and solves a generalized eigenvalue problem to estimate energies. Representative examples include quantum subspace expansion (QSE) [28], non-orthogonal VQE [29], and NOQE-style approaches that avoid on-device optimization [30]. Our recent generator-coordinate-inspired methods (GCIM) and adaptive variants further emphasize the need to repeatedly *add* basis states and re-evaluate matrix elements as the working subspace grows [31, 32]. Across such updates, the underlying state-preparation circuits typically differ only by which generators are activated and by their scalar coefficients, making them an ideal target for a compile-once, mask-aware execution model.

More broadly, many scientific workflows require *effective* descriptions obtained by integrating out high-energy degrees of freedom or restricting to a chemically relevant model space. In the Schrieffer–Wolff (SW) paradigm [33, 34] one seeks a near-identity unitary $e^{\hat{\sigma}}$ (with anti-Hermitian $\hat{\sigma}$) that approximately block-diagonalizes the Hamiltonian \hat{H} with respect to projectors P and $Q = 1 - P$, leading to an effective operator of the form $H_{\text{eff}} = P e^{-\hat{\sigma}} \hat{H} e^{\hat{\sigma}} P$ (and related projection-based variants) [35–37]. Such effective-Hamiltonian constructions underpin downfolding and embedding strategies across chemistry and materials science [38–42], including projector-based formalisms and canonical/similarity transformations. Importantly, SW can be viewed as a controlled low-order (or single-step) limit of *continuous* unitary flow-equation / similarity-renormalization approaches [43–45], where the generator and truncation masks are updated iteratively while the operator basis is kept structured. In these settings, the operator algebra may remain stable while only numerical data (coefficients, thresholds, or masks) changes across a family of related instances.

At the heart of many quantum algorithms for chemistry and many-body physics lies Hamiltonian simulation: the problem of encoding and evolving a high-dimensional operator with controlled error and resource overhead. Foundational approaches such as linear-combination-of-unitaries methods, quantum phase estimation, and qubitization have established optimal asymptotic bounds and motivated the modern framework of block encoding and polynomial spectral transformations, including quantum signal processing (QSP) and quantum singular value transformation (QSVT) [46–53]. Product-formula (Trotter–Suzuki) simulation remains an important complementary approach, with modern commutator-scaling error analyses [54]. Subsequent work has extended these ideas to fault-tolerant settings, structured Hamiltonians, and spectrum amplification techniques, further reinforcing block encoding as a unifying abstraction layer between physics and hardware [55–58].

In parallel, a large body of work has focused on reducing constant factors by exploiting physical structure in electronic-structure Hamiltonians. It is now well established that molecular Hamiltonians admit aggressive low-rank factorizations of the two-electron tensor, including pivoted Cholesky decompositions, tensor hypercontraction, and nested singular-value decompositions [59–69]. These representations compress the Hamiltonian into collections of rank-one or low-rank operators whose total count scales nearly linearly with system size for chemically relevant thresholds, enabling deterministic, number-conserving circuit constructions based on Givens rotations and fermionic swap networks [70–72].

Related low-rank structure also arises in correlated wavefunction methods. Coupled-cluster and unitary coupled-cluster generators, particularly at the doubles level, can be reshaped and factorized into rank-one excitation channels using singular-value and eigen-decomposition techniques [28, 73–77]. These decompositions reveal a shared algebraic backbone between Hamiltonians and similarity-transformation generators, suggesting that both objects can be treated within a unified operator-encoding framework. At the same time, perturbative methods such as MP2 [78, 79] often capture the dominant excitation subspaces at low cost, providing natural guidance for truncation, screening, and adaptive refinement strategies.

Despite these advances, most existing quantum simulation workflows still treat each block encoding as an instance-specific artifact. Changes in molecular geometry, basis set, active space, or truncation thresholds typically require recompiling large portions of the circuit, even when the underlying operator algebra is unchanged. This recompilation

overhead complicates geometry scans, active-space growth, and adaptive downfolding strategies, and obscures the separation between circuit topology and numerical data that is central to scalable quantum software design [80–84]. The conceptual reformulation pursued here—shifting from flat circuit execution to explicit operator-level structure control—is illustrated schematically in Figure 1.

Meanwhile, several end-to-end quantum simulation frameworks have emerged that aim to integrate state preparation, Hamiltonian encoding, and time evolution into cohesive pipelines suitable for early fault-tolerant devices [16, 17]. These efforts emphasize that state preparation and data access can be resource drivers comparable to Hamiltonian simulation itself, motivating continued work on deterministic loading schemes, eigenstate preparation, and efficient amplitude encoding [85–87]. However, these frameworks typically optimize resource counts for a given problem instance, whereas how to preserve a fixed logical circuit topology across a sequence of related instances encountered in geometry scans, active-space growth, or adaptive similarity transformations is still an unexplored area. In particular, the explicit decoupling of fixed circuit topology from instance-dependent numerical parameters is often implicit rather than an architectural principle.

This work addresses that gap by introducing **COMPOSER** (Compile-Once Modular Parametric Oracle for Similarity-Encoded Effective Reduction), a block-encoding architecture designed to explicitly separate circuit topology from numerical data. From an SW perspective, **COMPOSER** provides a compile-once execution stack for repeatedly constructing and updating block encodings of effective Hamiltonians induced by masked similarity transformations and projected model spaces. Starting from nested low-rank factorizations of molecular Hamiltonians and anti-Hermitian similarity generators, **COMPOSER** reduces both objects to linearly scaling collections of rank-one bilinear and projected-quadratic ladders. Each ladder is implemented using a deterministic, number-conserving adaptor circuit and wrapped into a single-ancilla block encoding. These adaptors are assembled within a fixed **PREP–SELECT–PREP**[†] skeleton whose two-qubit connectivity and ancilla usage are synthesized once and then frozen. For any supplied set of coefficients and masks, the resulting block-encoding and polynomial-approximation errors are systematically controllable via factorization thresholds, rotation precision, and polynomial degree.

We emphasize that **COMPOSER** is not a new Hamiltonian-simulation algorithm in the asymptotic sense. Instead, it is an architectural execution model for block-encoded chemistry operators: the two-

qubit multiplexing, routing, and signal-processing skeleton is synthesized once and then reused verbatim, while updates to molecular geometry, basis/active space choices, and classical truncation masks enter only through re-dialed single-qubit rotations and classical control data.

Although many block-encoding constructions reuse a generic PREP-SELECT-PREP[†] scaffold, the *compile-once* claim in COMPOSER is about *topology invariance across a family of related down-folded problems*: a single compiled two-qubit fabric supports geometry updates, active-space/model-space masks, and generator truncation masks inside a similarity-sandwiched effective Hamiltonian. This is enabled by three coupled design choices: (1) a *mask-aware similarity sandwich* that treats $P^{(m)}e^{-\hat{\sigma}^{(m)}}\hat{H}e^{\hat{\sigma}^{(m)}}P^{(m)}$ as the primary encoded object; (2) a *shared rank-one ladder operator language* for both \hat{H} and $\hat{\sigma}$, so the same adaptor bank applies to Hamiltonians and generators; and (3) *deterministic, number-conserving ladder realizations* (Givens/pair-Givens plus fixed routing) whose two-qubit pattern is fixed once an orbital pool and pivot choices are fixed. As a result, instance dependence is isolated to streamed coefficients and single-qubit rotation angles, while the selector tree, adaptor wiring, and QSP scaffold are compiled once and reused verbatim.

The current “compile-once” direction directly targets the problems encountered in related approaches. For example, in qROM/data-lookup LCU implementations, the data-access structure (e.g., qROM layout and its multiplexers) is typically built for a specific coefficient table; changing truncation patterns or term lists commonly triggers rebuilding the data-loading circuitry even when the high-level template is unchanged [87]. In Pauli-sum/Trotter pipelines, instance updates change the Pauli list and its grouping/ordering, so simulation and measurement circuits are regenerated and re-routed [54]. In variational settings, “compile-once” can refer to a fixed ansatz skeleton with updated parameters, but this targets state-preparation circuits and does not by itself enforce oracle-level topology invariance under active-space and similarity-generator masks [22, 24].

While the qubitization- and LCU-based constructions establish optimal asymptotic query and gate complexities for fixed Hamiltonians, they typically treat each block encoding as an instance-specific object whose circuit realization is synthesized for a particular operator decomposition. In contrast, COMPOSER promotes topology invariance to a design principle: the multiplexed two-qubit circuit fabric implementing the block encoding is compiled once, and subsequent changes in operator coeffi-

cients, truncation masks, or active spaces are absorbed entirely into updated single-qubit parameters and classical selector data.

Within this fixed topology, all instance dependence—including molecular geometry, basis choice, active-space expansion, truncation masks, and similarity-transformation targets—enters solely through single-qubit rotation angles. Importantly, these angles need not be sourced from coupled-cluster amplitudes: for Hamiltonian block encodings they are typically determined by numerically controlled integral factorizations (e.g., Cholesky/density fitting/tensor hyper-contraction ranks and thresholds), while coupled-cluster or tensor-network amplitudes provide only one convenient *initialization* for optional similarity generators or masking heuristics. For any fixed choice of encoded operators, the residual block-encoding and QSP approximation errors are independently and systematically controllable via factorization rank/thresholds, rotation precision, and polynomial degree. If all angles are sourced from a classical approximate object and never refined, then the achievable physical accuracy is ultimately bounded by that approximation even when the algorithmic simulation error is tunable. A single quantum signal processing polynomial implements time evolution (and more general spectral transformations) for the resulting masked operator sums, with polynomial degree determined by spectral norms rather than term count [88, 89]. Similarity updates enter through re-parameterizing the encoded operator (the mask-aware similarity-sandwich), not by treating conjugation itself as a spectral function of the Hamiltonian. This compile-once, tune-many design enables adaptive workflows with predictable resource bounds while eliminating recompilation of the fixed two-qubit circuit topology across closely related problem instances, with only single-qubit parameters updated between instances.

The focus of this work is the construction and reuse of a fixed-topology block-encoding architecture—and the resulting mask-aware, compile-once execution model—rather than proposing a new simulation primitive or reporting end-to-end chemical accuracy benchmarks. We introduce deterministic rank-one adaptor circuits, develop a mask-aware similarity-sandwich construction for effective Hamiltonians, analyze depth and ancilla tradeoffs, and validate the stability of the underlying rank-one operator structure using numerical experiments and MP2-guided subspace selection. Together, these elements establish COMPOSER as a hardware-native block-encoding framework that supports efficient adaptive quantum simulation in both NISQ demonstrations and early

fault-tolerant regimes.

II. RANK-ONE REPRESENTATIONS OF QUANTUM-CHEMISTRY OPERATORS

Throughout this section we use standard second-quantized notation for fermionic creation and annihilation operators acting on an orthonormal spin-orbital basis of size M_{so} . The system register consists of $n = M_{\text{so}}$ qubits, while ancillary qubits are introduced only to realize block encodings, selector registers, and quantum signal processing (QSP) primitives. Rank-one operators are labeled by an index s , and collections of such operators are assembled using binary-addressed selector registers. A classical *mask* $\mathcal{M}^{(m)}$ specifies subsets of rank-one terms retained in truncated generators or effective Hamiltonians. Symbols used throughout the manuscript are summarized in Table I.

A. Rank-one operators

We begin by defining a common notion of *rank-one operators* in operator space, which will serve as the fundamental building blocks for Hamiltonians, similarity generators, and their block encodings throughout this work. We assume a standard second-quantized fermion-to-qubit encoding with one qubit per spin-orbital (e.g., Jordan–Wigner or parity mappings), so $n = M_{\text{so}}$. The deterministic number-conserving adaptors used later are built from Givens-rotation primitives and fermionic swap-network routing [70, 71].

Definition 1 (Rank-one bilinear operator). *Let $u, v \in \mathbb{C}^{M_{\text{so}}}$ be normalized single-particle coefficient vectors,*

$$u = (u_1, u_2, \dots, u_n)^\top, \quad v = (v_1, v_2, \dots, v_n)^\top, \quad (1)$$

with $\sum_{p=1}^n |u_p|^2 = 1$ and $\sum_{q=1}^n |v_q|^2 = 1$. $\lambda \in \mathbb{C}$ a scalar. Define the projected creation and annihilation operators

$$\hat{a}_u^\dagger = \sum_{p=1}^{M_{\text{so}}} u_p a_p^\dagger, \quad \hat{a}_v = \sum_{q=1}^{M_{\text{so}}} v_q^* a_q, \quad (2)$$

with the subscript u a label for the whole vector, not an orbital index, and set

$$\hat{L}^{(I)} = \lambda \hat{a}_u^\dagger \hat{a}_v. \quad (3)$$

The matrix elements $L_{pq} = \lambda u_p v_q^$ form an outer product of two length- M_{so} vectors. The term “rank-one” here refers to the outer-product structure of the*

coefficient tensor in the single-particle operator basis, not to the rank of the induced operator on the many-body Hilbert space.

Remark (canonical mode transformations). The linear redefinition of fermionic modes in Eq. (2) is a particle-number-conserving special case of a general fermionic canonical (Bogoliubov–Valatin) transformation [90, 91], obtained by restricting to transformations that do not mix creation and annihilation operators.

Definition 2 (Rank-one pair-excitation operator). *Let $U \in \mathbb{C}^{N_v \times N_v}$ and $V \in \mathbb{C}^{N_o \times N_o}$ be antisymmetric tensors on the virtual and occupied subspaces, respectively. Define the pair creation and annihilation operators*

$$\hat{B}^\dagger[U] = \sum_{a < b} U_{ab} a_a^\dagger a_b^\dagger, \quad \hat{B}[V] = \sum_{i < j} V_{ij}^* a_j a_i. \quad (4)$$

For $\lambda \in \mathbb{C}$, define

$$\hat{L}^{(II)} \equiv \lambda \hat{B}^\dagger[U] \hat{B}[V]. \quad (5)$$

Although \hat{L} is quartic in fermionic operators, it is rank-one in the composite pair-excitation index (ab, ij) , since its coefficient tensor factorizes as $L_{ab,ij} = \lambda U_{ab} V_{ij}$.

Remark. If $x, y \in \mathbb{C}^{N_v}$ and $r, s \in \mathbb{C}^{N_o}$, one may take $U_{ab} = (x_a y_b - x_b y_a) / \sqrt{2}$ and $V_{ij} = (r_i s_j - r_j s_i) / \sqrt{2}$, yielding $\hat{B}^\dagger[U] = a^\dagger(x) a^\dagger(y)$ and $\hat{B}[V] = a(s) a(r)$, where

$$a^\dagger(x) = \sum_a x_a a_a^\dagger, \quad a^\dagger(y) = \sum_b y_b a_b^\dagger, \quad (6)$$

$$a(s) = \sum_j s_j^* a_j, \quad a(r) = \sum_i r_i^* a_i. \quad (7)$$

Equivalently, U and V may be viewed as vectors in the antisymmetric pair spaces $\mathbb{C}^{N_v \times N_v}$ and $\mathbb{C}^{N_o \times N_o}$. This form directly maps to the two-electron deterministic ladders constructed in Sec. III B and also discussed in Refs. 70–72. Without loss of generality one may normalize u and v and absorb their norms into λ , which is convenient for deterministic state preparation.

Definition 3 (Projected quadratic rank-one operator). *This construction captures Jastrow-like [92] quadratic occupation operators in a rank-one form. Let $\{u^{(r)}\}_{r=1}^R \subset \mathbb{C}^{M_{\text{so}}}$ be a collection of single-particle coefficient vectors and define $\hat{a}^\dagger(u^{(r)}) = \sum_{p=1}^{M_{\text{so}}} u_p^{(r)} a_p^\dagger$ and $\hat{a}_r = \hat{a}^\dagger(u^{(r)}) \hat{a}(u^{(r)})$. For coefficients $\mathbf{C} = (C_1, \dots, C_R) \in \mathbb{C}^R$ define*

$$\hat{O} = \sum_{r=1}^R C_r \hat{a}_r, \quad (8)$$

$$\hat{L}^{(III)} = \hat{O} \hat{O}^\dagger. \quad (9)$$

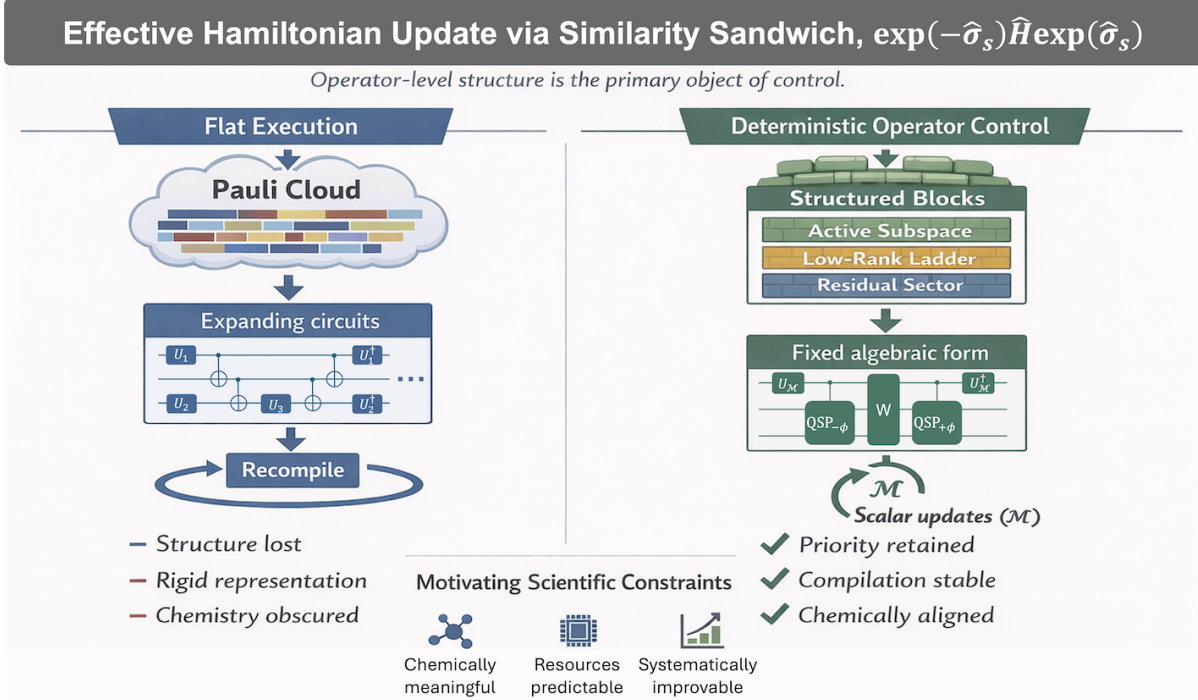


FIG. 1. Conceptual motivation for operator-level structure control. Conventional workflows flatten second-quantized operators (\hat{H} , \hat{T} , $\hat{\sigma}$, ...) into unstructured Pauli expansions, leading to expanding circuit constructions and repeated recompilation during iterative optimization or instance updates. In this flat execution paradigm, excitation hierarchy and chemically meaningful subspaces are obscured at the circuit level. In contrast, the COMPOSER architecture treats operator structure as the primary object of control. Nested low-rank factorizations yield structured blocks (e.g., active subspaces, low-rank ladders, residual sectors) that are embedded within a fixed algebraic topology. Instance dependence enters only through scalar parameter updates, enabling stable compilation and predictable resource scaling. This shift from gate-level optimization to operator-level control, implemented as a fixed-topology block-encoding architecture with streamed parameters, is guided by three motivating scientific constraints: preserving chemical meaning, ensuring predictable resource growth, and enabling systematic hierarchy refinement.

Although $\hat{L}^{(III)}$ expands into many quartic monomials, its coefficient matrix over the (r, r') index pair is the outer product $C_r C_r^*$, hence rank-one in that index space.

In what follows we write \hat{L} for any rank-1 ladder, omitting the superscripts (I) – (III); the appropriate type is determined by the accompanying index set (one-electron vs pair vs number-conserving) and the surrounding discussion.

B. Rank-one representation of the molecular Hamiltonian

This subsection shows that the molecular Hamiltonian can be organized as a linear combination of rank-one operator ladders whose *count* is empirically near-linear in M_{so} at fixed integral-factorization thresholds.

The electronic Hamiltonian in second quantiza-

tion is

$$\hat{H} = \sum_{pq} h_{pq} a_p^\dagger a_q + \frac{1}{2} \sum_{pqrs} \langle pq|rs \rangle a_p^\dagger a_q^\dagger a_s a_r + E_{\text{nn}}. \quad (10)$$

We use the physicist's (non-antisymmetrized) two-electron integrals $\langle pq|rs \rangle$, since fermionic antisymmetry is enforced by operator ordering and this form is directly amenable to Cholesky factorization. The nuclear-repulsion constant E_{nn} contributes only an overall energy shift and may therefore be dropped or tracked separately.

Applying a pivoted Cholesky decomposition to the two-electron tensor yields [59–64]

$$\langle pq|rs \rangle \approx \sum_{\mu=1}^K L_{pr}^\mu L_{qs}^\mu, \quad (11)$$

where each L^μ is an $M_{\text{so}} \times M_{\text{so}}$ symmetric matrix and K is chosen according to a prescribed threshold. Related integral-compression approaches such as den-

Symbol	Meaning
M_{so}	# spin-orbitals in the chosen basis
n	# qubits in the <i>system</i> register ($n = M_{\text{so}}$)
N_O, N_V	# occupied and virtual spin orbitals in the chosen active space
a^\dagger, a	Fermionic creation/annihilation operators
\hat{a}^\dagger, \hat{a}	Linear combination of Fermionic creation/annihilation operators
λ	Complex prefactor of a rank-one operator
\hat{L}_s	Rank-one operator
$\hat{A}_s = \hat{L}_s - \hat{L}_s^\dagger$	anti-Hermitian rank-one term
$\hat{\Lambda}_s = i(\hat{L}_s - \hat{L}_s^\dagger)$	Hermitian rank-one term
$\omega_s, \Omega_s \in \mathbb{R}$	Real coefficient of a rank-one operator
ℓ_H	# rank-one operators in Hamiltonian factorization
ℓ_σ	# rank-one terms in anti-Hermitian operator $\hat{\sigma}$
$\mathcal{M}^{(m)}$	Classical <i>mask</i> selecting labels s
α	Normalization constant of a block encoding
$a = \max(\lceil \log_2 \ell_H \rceil, \lceil \log_2 \ell_\sigma \rceil)$	Selector-register width
d	Quantum signal processing (QSP) polynomial degree
$U_{\text{prep}}, W_{\text{sel}}$	PREP loader and SELECT cascade

TABLE I. Summary of notation and key algebraic symbols used in the COMPOSER framework and rank-one block-encoding constructions. Unless otherwise stated we absorb phases into single-particle vectors so that Hamiltonian and generator weights (Ω_s, ω_s) may be taken real.

sity fitting / resolution-of-the-identity and tensor hypercontraction provide alternative low-rank representations of the same two-electron tensor and have been widely used in classical electronic-structure theory [65, 66, 93]. After the standard mean-field shift

$$\tilde{h}_{pq} = h_{pq} - \frac{1}{2} \sum_s \langle pq | ss \rangle, \quad (12)$$

both \tilde{h} and each Cholesky factor L^μ may be diagonalized in their respective single-particle bases. Note that the diagonalizing rotation is generally μ -dependent, so the operators $\hat{n}_{\mu\xi}$ below live in different one-particle bases for different μ .

Rewriting the Hamiltonian in the resulting rotated orbitals yields [11, 64, 68, 69]

$$\hat{H} = \sum_{\eta=1}^{R_1} \kappa_\eta \hat{a}_\eta^\dagger \hat{a}_\eta + \frac{1}{2} \sum_{\mu=1}^K \left(\sum_{\xi=1}^{R_\mu} \lambda_\xi^\mu \hat{n}_{\mu\xi} \right)^2, \quad (13)$$

Here $R_1 \leq M_{\text{so}}$ denotes the number of retained eigenmodes of \tilde{h} after optional truncation; without truncation $R_1 = M_{\text{so}}$. Similarly, R_μ is determined by the retained spectral rank of the μ th factor after thresholding. \hat{a}_η^\dagger and $\hat{n}_{\mu\xi}$ denote creation and occupation operators in the corresponding rotated bases. Importantly, both the one-electron and two-electron contributions are expressed using the same rank-one ladder structure introduced in Sec. II A. In particular, for each Cholesky channel μ we define the

diagonal one-body operator

$$\hat{O}_\mu := \sum_{\xi=1}^{R_\mu} \lambda_\xi^{(\mu)} \hat{n}_{\mu\xi}, \quad (14)$$

so that the channel contribution is the *projected quadratic rank-one* operator

$$\hat{L}_\mu := \hat{O}_\mu \hat{O}_\mu^\dagger = \hat{O}_\mu^2, \quad (15)$$

which is precisely of the form in **Definition 3** with coefficient vector $C = \lambda^{(\mu)}$.

Collecting terms, the Hamiltonian may therefore be written compactly as

$$\hat{H} = \sum_{s=1}^{\ell_H} \Omega_s \hat{L}_s, \quad (16)$$

where each \hat{L}_s is a rank-one operator and

$$\ell_H = R_1 + K. \quad (17)$$

For a fixed Cholesky threshold, empirical studies typically find that K (and hence ℓ_H) grows approximately linearly with M_{so} for a wide range of molecular systems [56, 68], which is the key structural property that enables fixed-topology block encodings in the COMPOSER architecture.

C. Rank-one representation of the cluster generator

We now show that the anti-Hermitian coupled-cluster doubles generator admits a rank-one decomposition compatible with the operator ladders introduced in Sec. II A. Throughout this subsection we

adopt the convention that occupied and virtual indices are explicitly antisymmetrized.

We focus on the doubles excitation operator,

$$\hat{T}_2 = \sum_{a < b} \sum_{i < j} t_{ab,ij} a_a^\dagger a_b^\dagger a_j a_i, \quad (18)$$

where (i, j) label occupied spin-orbitals and (a, b) label virtual spin-orbitals in an orthonormal spin-orbital basis. Singles contributions are inherently rank-one and may be treated analogously; higher-order excitations can be incorporated using the same principles.

To expose low-rank structure while respecting fermionic antisymmetry, we view $t_{ab,ij}$ as a matrix on antisymmetric pair spaces by introducing composite indices $ab \equiv (a < b)$ and $ij \equiv (i < j)$, so that $t_{ab,ij}$ is a $\binom{N_V}{2} \times \binom{N_O}{2}$ matrix. Equivalently, for each μ the factors below may be unpacked as skew-symmetric tensors $\mathbb{M}_{ab}^{(\mu)} = -\mathbb{M}_{ba}^{(\mu)}$ and $\mathbb{N}_{ij}^{(\mu)} = -\mathbb{N}_{ji}^{(\mu)}$. We then perform a singular-value decomposition [28, 73–77],

$$t_{ab,ij} = \sum_{\mu=1}^{R_\mu} \epsilon_\mu \mathbb{M}_{ab}^{(\mu)} \mathbb{N}_{ij}^{(\mu)}, \quad (19)$$

where the upper limit R_μ is determined by a prescribed truncation threshold for T_2 .

Each singular component is then further expressed as a sum of *rank-one antisymmetric pair factors* (wedge products) within its respective subspace. Concretely, we approximate

$$\mathbb{M}_{ab}^{(\mu)} \approx \sum_{\kappa=1}^{R_\kappa} \epsilon_\kappa^{(\mu)} U_{ab}^{(\mu\kappa)}, \quad (20)$$

$$\mathbb{N}_{ij}^{(\mu)} \approx \sum_{\eta=1}^{R_\eta} \epsilon_\eta^{(\mu)} V_{ij}^{(\mu\eta)}, \quad (21)$$

where

$$U_{ab}^{(\mu\kappa)} = \frac{x_a^{(\mu\kappa)} y_b^{(\mu\kappa)} - x_b^{(\mu\kappa)} y_a^{(\mu\kappa)}}{\sqrt{2}}, \quad (22)$$

$$V_{ij}^{(\mu\eta)} = \frac{r_i^{(\mu\eta)} s_j^{(\mu\eta)} - r_j^{(\mu\eta)} s_i^{(\mu\eta)}}{\sqrt{2}}, \quad (23)$$

where the antisymmetry $U_{ab}^{(\mu\kappa)} = -U_{ba}^{(\mu\kappa)}$ and $V_{ij}^{(\mu\eta)} = -V_{ji}^{(\mu\eta)}$ is explicit. (The factor of $1/\sqrt{2}$ is a convention; it may be absorbed into the vectors or coefficients depending on the chosen normalization of the pair basis.) This yields the explicit factorization

$$t_{ab,ij} \approx \sum_{\mu,\kappa,\eta} \epsilon_\mu \epsilon_\kappa^{(\mu)} \epsilon_\eta^{(\mu)} U_{ab}^{(\mu\kappa)} V_{ij}^{(\mu\eta)}. \quad (24)$$

Employing the definition of the pair creation/annihilation operators in Eq. (4), we can write the rank-one pair-excitation ladder as

$$\hat{L}_{\mu,\kappa,\eta} \equiv \hat{B}^\dagger [U^{(\mu\kappa)}] \hat{B} [V^{(\mu\eta)}]. \quad (25)$$

The doubles operator therefore admits the rank-one expansion

$$\hat{T}_2 \approx \sum_{\mu,\kappa,\eta} \omega_{\mu,\kappa,\eta} \hat{L}_{\mu,\kappa,\eta} \quad (26)$$

with $\omega_{\mu,\kappa,\eta} := \epsilon_\mu \epsilon_\kappa^{(\mu)} \epsilon_\eta^{(\mu)}$. The corresponding anti-Hermitian generator is

$$\begin{aligned} \hat{\sigma}_2 &= \hat{T}_2 - \hat{T}_2^\dagger \\ &\approx \sum_{\mu,\kappa,\eta} \omega_{\mu,\kappa,\eta} \left(\hat{L}_{\mu,\kappa,\eta} - \hat{L}_{\mu,\kappa,\eta}^\dagger \right), \end{aligned} \quad (27)$$

a structured sum of rank-one ladders. Phases may be absorbed into the orbital vectors so that $\omega_{\mu,\kappa,\eta} \in \mathbb{R}$, making each $\omega_{\mu,\kappa,\eta} (\hat{L} - \hat{L}^\dagger)$ manifestly anti-Hermitian.

This representation makes explicit that the coupled-cluster generator is built from the same algebraic primitives as the Hamiltonian decomposition in Sec. II B. As a result, Hamiltonians and similarity generators can be treated on equal footing within the COMPOSER block-encoding architecture.

III. DETERMINISTIC PREPARATION OF ONE- AND TWO-ELECTRON STATES

In this section we construct deterministic ladder circuits that realize the rank-one operators introduced in Sec. II. The core objects are number-conserving ladder unitaries U_u built from Givens (and pair-Givens) rotations, optional routing swaps, and diagonal phase shifts. These ladders serve a dual role: when preceded by a simple pivot injection and applied to the vacuum, they prepare one- and two-electron states with prescribed amplitudes; when applied without injection, they act as basis-rotation primitives inside rank-one block-encoding adaptors. The same fixed ladder topology is reused throughout the COMPOSER architecture.

A. Deterministic preparation of the one-electron state

The target state in the one-electron sector is

$$|u\rangle = \hat{a}_u^\dagger |0^n\rangle = \sum_{p=1}^n u_p |p\rangle, \quad (28)$$

where $|p\rangle = a_p^\dagger|0^n\rangle$ with $p \in \{1, \dots, n\}$ denotes the Slater determinant with the p th spin-orbital occupied.

We construct a deterministic preparation circuit by composing (i) a single-electron pivot injection and (ii) a number-conserving ladder unitary. Concretely, fix a pivot orbital r (chosen once to define a fixed ladder topology) and define $|r\rangle = X_r|0^n\rangle$. We then build a number-conserving unitary U_u from two-mode Givens rotations and diagonal phase shifts such that $U_u|r\rangle = |u\rangle$, so that the full preparation circuit is $U_{\text{prep}}^{(u)} = U_u X_r$ [70–72]. For numerical stability one may choose r so that $|u_r|$ is not anomalously small (e.g., $r = \arg \max_p |u_p|$), but this is not required for correctness; it only affects the conditioning of the classical angle recursion.

For each $p \neq r$, the number-conserving Givens rotation is defined as

$$G_{pr}(\theta) = \exp[\theta (a_p^\dagger a_r - a_r^\dagger a_p)], \quad (29)$$

which acts as an SO(2) rotation on $\text{span}\{|r\rangle, |p\rangle\}$. A fixed ordering of the non-pivot orbitals defines a ladder that sequentially transfers amplitude out of the pivot mode; the required rotation angles and residual single-qubit phases are computed classically from u . Here the data vector u (and similarly u_{pq} in the two-electron ladder) is supplied by the chosen operator factorization/parameterization—e.g., integral-derived low-rank factors for \hat{H} or solver-seeded factors for $\hat{\sigma}$ —and is not restricted to coupled-cluster doubles. Explicit recursions and an explicit product form are collected in Appendix A. The resulting circuit prepares $|u\rangle$ deterministically; its inverse is obtained by reversing the gate order and negating all angles. The one-electron ladder uses $(n-1)$ two-mode rotations (plus phases and optional routing swaps), so its gate count scales as $\mathcal{O}(n)$ for fixed connectivity assumptions.

Remark (number-conserving form). By construction U_u is strictly number-conserving (it preserves each fixed- N sector); the preparation form differs only by the initial pivot injection X_r . This is the form reused inside rank-one block-encoding adaptors, independent of whether the system register holds the vacuum or an arbitrary N -electron state.

B. Deterministic preparation of a two-electron state

The two-electron ladder generalizes Sec. III A to antisymmetric excitation pairs [70–72]. Let $u_{pq} = -u_{qp}$ be a normalized antisymmetric coefficient tensor, $\sum_{p<q} |u_{pq}|^2 = 1$. The target state in the two-

electron sector is

$$|u\rangle = \sum_{p<q} u_{pq} |pq\rangle, \quad |pq\rangle = a_p^\dagger a_q^\dagger |0^n\rangle. \quad (30)$$

Fix a pivot pair (r, s) with $r < s$ (chosen once to define a fixed ladder topology) and inject two particles,

$$X_r X_s |0^n\rangle = |rs\rangle. \quad (31)$$

Here, as in the one-electron case, choosing (r, s) so that $|u_{rs}|$ is not anomalously small improves the conditioning of the classical angle/phase recursion but is not required for correctness. Amplitude is then redistributed from the pivot pair using phased pair-Givens rotations. For each unordered pair $\{p, q\} \neq \{r, s\}$, define

$$G_{pq,rs}(\theta, \phi) = \exp\left[\theta(e^{i\phi} a_p^\dagger a_q^\dagger a_s a_r - e^{-i\phi} a_r^\dagger a_s^\dagger a_q a_p)\right], \quad (32)$$

which preserves particle number and rotates $\text{span}\{|rs\rangle, |pq\rangle\}$. As in the one-electron case, a fixed ordering of non-pivot pairs defines a deterministic ladder; angles and phases are computed classically from $\{u_{pq}\}$ (Appendix A). Equivalently, define the number-conserving ladder U_u such that $U_u|rs\rangle = |u\rangle$, so the full preparation circuit is $U_{\text{prep}}^{(u)} = U_u X_r X_s$. The two-electron ladder contains one pair rotation per non-pivot pair (up to ordering/truncation), i.e., $\binom{n}{2} - 1$ rotations in the worst case, so its size scales as $\mathcal{O}(n^2)$ before sparsity/truncation and connectivity-aware compilation.

Remark (number-conserving form). Omitting the initial excitation $X_r X_s$ yields a strictly number-conserving ladder unitary U_u that acts as a basis rotation within the two-electron subspace. This number-conserving form is the one used inside pair-excitation adaptors in COMPOSER.

Preparation vs. number conservation. Throughout the remainder of this work, U_u denotes the number-conserving ladder form. When needed we disambiguate by writing $U_u^{(1)}$ (one-electron ladder) and $U_u^{(2)}$ (two-electron ladder); otherwise the intended sector is clear from context. The preparation form from the vacuum differs only by the initial pivot injection (one X gate for the one-electron ladder; two X gates for the two-electron ladder). For completeness, we collect explicit product decompositions and a short discussion of these two realizations, as well as connectivity-aware routing, Givens-SWAP network constructions, and depth scaling for the two-electron ladders, in Appendix A.

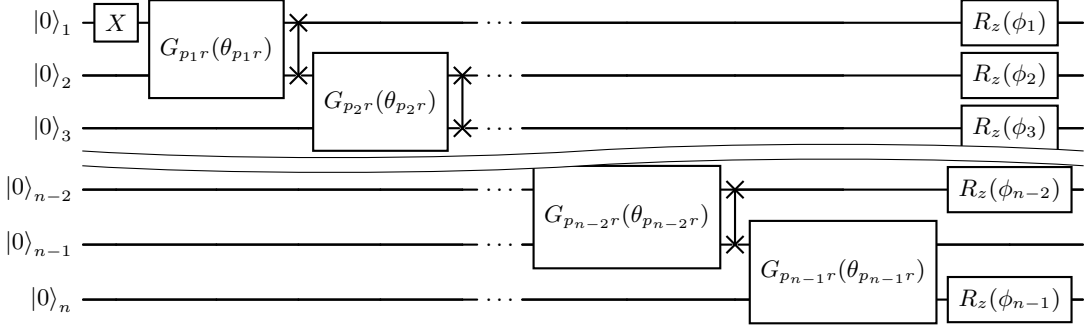


FIG. 2. Deterministic ladder circuit for one-electron state preparation. The ladder topology is fixed; only the angles $\{\theta_{pr}\}$ and phases $\{\phi_p\}$ depend on the data vector u (see Appendix A). The interleaved swaps indicate a connectivity-aware routing pattern; when the ladder is used as a basis rotation on general N -electron states, these swaps should be interpreted as fermionic swap-network primitives (or an equivalent orbital-routing compilation) [70].

IV. BLOCK ENCODING OF RANK-ONE OPERATORS

COMPOSER is formulated on an n -qubit second-quantized register, but its oracles are used only on a fixed particle-number sector $\mathcal{H}_{N_e} \subset (\mathbb{C}^2)^{\otimes n}$ (and, when indicated, on a user-chosen model subspace $\text{Ran}(P^{(m)}) \subseteq \mathcal{H}_{N_e}$). All ladder primitives and adaptor branches used in COMPOSER are strictly number conserving (Sec. III and Appendix A), so \mathcal{H}_{N_e} is an invariant subspace of every SELECT branch and of the assembled PREP-SELECT-PREP[†] circuits.

Accordingly, throughout this section, statements of the form $(\langle 0^t | \otimes I) W_{\hat{O}} (|0^t \rangle \otimes I) \approx \hat{O}/\alpha$ are to be understood as holding in operator norm *after restriction to the working subspace*. That is, for Π_{N_e} the orthogonal projector onto \mathcal{H}_{N_e} , we require

$$\|\Pi_{N_e} [(\langle 0^t | \otimes I) W (|0^t \rangle \otimes I) - \hat{O}/\alpha] \Pi_{N_e}\| \leq \epsilon.$$

Outside the working subspace (e.g., on other Hamming-weight sectors), the action of the block-encoding unitary is unconstrained and irrelevant to COMPOSER's use cases. For readability we suppress the explicit Π_{N_e} sandwiches in most equations below.

A. Encoding rank-one operators

Lemma 1 (Single-ancilla dyad block encoding in the one-excitation register). *Throughout this lemma we treat $\hat{a}_u^\dagger \hat{a}_v$ as an operator restricted to the embedded one-electron subspace $\mathcal{H}_{N=1} \subset (\mathbb{C}^2)^{\otimes n}$, on which it is exactly the dyad $|u\rangle\langle v|$. Let $\hat{L}_s = \lambda_s \hat{a}_u^\dagger \hat{a}_v$ be a bilinear rank-one operator (Eq. (3)) with $u, v \in \mathbb{C}^n$ and $\lambda_s \in \mathbb{C}$. In this lemma we consider the induced action on the single-excitation subspace $\mathcal{H}_1 \subset (\mathbb{C}^2)^{\otimes n}$, where $\hat{a}_u^\dagger \hat{a}_v$ acts exactly as the dyad $|u\rangle\langle v|$.*

Without loss of generality, phases may be absorbed into u and v so that $\lambda_s \in \mathbb{R}_{\geq 0}$. For any error $\epsilon > 0$, there exists a unitary W_s acting on the system and one ancilla qubit such that

$$\|(\langle 0 | \otimes I_S) W_s (|0 \rangle \otimes I_S) - \hat{L}_s/\alpha\| < \epsilon, \quad (33)$$

with normalization $\alpha \geq |\lambda_s|$.

Proof. See Appendix B.

Remark 1. In the many-electron use cases of COMPOSER, the same ladder primitives U_u, U_v appear as number-conserving orbital-rotation subroutines inside the full SELECT table; the dyad viewpoint is used here only to give a compact correctness proof of the rank-one adaptor interface.

Remark 2. Based on Lemma 1, we can further block encode the the pair-excitation ladder $\hat{B}^\dagger[U]\hat{B}[V]$. We denote $\hat{L}_s = \lambda_s \hat{B}^\dagger[U]\hat{B}[V]$ as a rank-one pair-excitation operator with antisymmetric pair tensors U, V , and $\lambda_s \in \mathbb{C}$. Assume U and V are normalized in the antisymmetric pair basis, $\sum_{p<q} |U_{pq}|^2 = 1$, $\sum_{p<q} |V_{pq}|^2 = 1$, and define the corresponding normalized two-electron states $|U\rangle := \hat{B}^\dagger[U]|0^n\rangle$, $|V\rangle := \hat{B}^\dagger[V]|0^n\rangle$. Then on $\mathcal{H}_{N=2} \subset (\mathbb{C}^2)^{\otimes n}$, the operator $\hat{B}^\dagger[U]\hat{B}[V]$ acts exactly as the dyad $|U\rangle\langle V|$. Without loss of generality, $\arg(\lambda_s)$ can be absorbed into U or V so that $\lambda_s \in \mathbb{R}_{\geq 0}$. For any error $\epsilon > 0$, there exists a unitary W_s acting on the system register and one ancilla qubit such that Eq. (33) holds. In the many-electron use cases of COMPOSER, the same two-electron ladder primitives from Sec. III B appear in their number-conserving form inside the SELECT table; the restriction to $\mathcal{H}_{N=2}$ is used here only to state a compact adaptor-correctness interface, analogous to Lemma 1.

Lemma 2 (Deterministic block encoding of a squared diagonalized Cholesky channel). Let $L^\mu \in \mathbb{C}^{n \times n}$ be a (single-bar) Cholesky channel with eigen-decomposition $L^\mu = U^{(\mu)} \text{diag}(\lambda^{(\mu)}) U^{(\mu)\dagger}$. Define rotated modes $\hat{a}_{\mu\xi}^\dagger = \sum_p U_{p\xi}^{(\mu)} \hat{a}_p^\dagger$ and $\hat{n}_{\mu\xi} = \hat{a}_{\mu\xi}^\dagger \hat{a}_{\mu\xi}$, and define the Hermitian operator

$$\hat{O}_\mu := \sum_{\xi=1}^{R_\mu} \lambda_\xi^{(\mu)} \hat{n}_{\mu\xi}, \quad \Gamma_\mu := \sum_{\xi=1}^{R_\mu} |\lambda_\xi^{(\mu)}|. \quad (34)$$

Then \hat{O}_μ^2 admits a deterministic $(\Gamma_\mu^2, \mathbf{a}_I + 2, 0)$ block encoding, where \mathbf{a}_I is the width of the index register (binary: $\mathbf{a}_I = \lceil \log_2 R_\mu \rceil$; unary: $\mathbf{a}_I = R_\mu$). Concretely, we first construct a deterministic block encoding of \hat{O}_μ/Γ_μ using PREP-SELECT-PREP[†] over the commuting projectors $\{\hat{n}_{\mu\xi}\}$ (including the sign of $\lambda_\xi^{(\mu)}$ as a branch phase), and then apply a fixed, degree-2 QSVT/QSP polynomial implementing $x \mapsto x^2$ to obtain $\hat{O}_\mu^2/\Gamma_\mu^2$.

Proof. See Appendix B.

General remark (two types of rank-one adaptors). Lemmas 1 and 2 implement two complementary rank-one block-encoding primitives. Lemma 1 encodes a bilinear rank-one operator $\hat{L} = \lambda \hat{a}_u^\dagger \hat{a}_v$, which couples two distinct single-particle modes and is realized using deterministic one-electron state-preparation ladders. In the double-factorized form, each Cholesky channel contributes $\frac{1}{2} \hat{O}_\mu^2$ with $\hat{O}_\mu = \sum_\xi \lambda_\xi^{(\mu)} \hat{n}_{\mu\xi}$; Lemma 2 provides a deterministic adaptor for \hat{O}_μ and, via a fixed degree-2 QSVT step, for \hat{O}_μ^2 without enumerating the $\mathcal{O}(R_\mu^2)$ cross terms explicitly. Together, these two adaptors span the bilinear and quadratic building blocks arising from the nested factorization of molecular Hamiltonians and cluster generators, and both admit deterministic, single-signal block encodings with fixed circuit topology.

Theorem 1 (Binary-multiplexed block encoding). Suppose $\hat{H} = \sum_{s=1}^{\ell_H} \Omega_s \hat{L}_s$ and for each s there exists a unitary W_s that is an $(\alpha_s, t, \epsilon_s)$ block encoding of \hat{L}_s , acting on an n -qubit system register with t ancillas initialized in $|0^t\rangle$. Then there exists a unitary W that is an $(\alpha, \mathbf{a}_H + t, \epsilon_{\text{LCU}})$ block encoding of \hat{H} such that

$$\left\| \left(\langle 0^{\mathbf{a}_H+t} | \otimes I_S \right) W \left(|0^{\mathbf{a}_H+t}\rangle \otimes I_S \right) - \frac{\hat{H}}{\alpha} \right\| < \epsilon_{\text{LCU}}, \quad (35)$$

where

$$\alpha = \sum_{s=1}^{\ell_H} |\Omega_s| \alpha_s, \quad \epsilon_{\text{LCU}} = \frac{1}{\alpha} \sum_{s=1}^{\ell_H} |\Omega_s| \alpha_s \epsilon_s.$$

Here $\mathbf{a}_H = \lceil \log_2 \ell_H \rceil$ is the selector width, and the t ancillas used by W_s are reused across all branches [48, 49, 51, 52]. The corresponding binary-multiplexed PREP-SELECT-PREP[†] circuit structure is shown in Figure 3.

The circuit depth obeys

$$\text{depth}(W) = \mathcal{O} \left(\text{depth}(U_{\text{prep}}) + \sum_{s=1}^{\ell_H} \text{depth}(c-W_s) \right).$$

Here $\text{depth}(c-W_s)$ denotes the depth of the selector-controlled implementation of W_s . For example, W_s may be constructed using Lemma 1 (bilinear adaptor) or Lemma 2 (diagonal Cholesky-channel adaptor), leading to representative costs $\text{depth}(W_s) = \mathcal{O}(n)$ and $\text{depth}(W_s) = \mathcal{O}(n + R_\mu)$, respectively, where R_μ is the number of retained rotated modes in channel μ .

Proof. See Appendix B.

B. Encoding exponentials of rank-one generators

We now describe how to implement the exponential of an anti-Hermitian generator,

$$\hat{\sigma} = \sum_{s=1}^{\ell_\sigma} \omega_s \hat{A}_s, \quad \hat{A}_s = \hat{L}_s - \hat{L}_s^\dagger, \quad (36)$$

where each \hat{L}_s is a rank-one operator and $\omega_s \in \mathbb{R}$. Defining the associated Hermitian operators

$$\hat{\mathbb{A}}_s := i \hat{A}_s, \quad (37)$$

we may rewrite

$$e^{\hat{\sigma}} = e^{-i \sum_s \omega_s \hat{\mathbb{A}}_s}. \quad (38)$$

We emphasize that QSP is applied only to the block encoding of the generator $\hat{\sigma}$. The Hamiltonian block encoding constructed in Sec. IV A is not exponentiated and therefore does not incur polynomial-degree overhead.

a. Block encoding of the generator. Using Lemma 1 and Theorem 1, each $\hat{\mathbb{A}}_s$ admits a $(2\alpha_s, 1, 2\epsilon_s)$ block encoding $W_{\hat{\mathbb{A}}_s}$, where the factor of 2 accounts for \hat{L}_s and \hat{L}_s^\dagger . Applying the PREP-SELECT-PREP[†] construction yields a block encoding of the full generator,

$$U_{\hat{\sigma}} = (U_{\text{prep}}^\dagger \otimes I) \left(\sum_{s=1}^{\ell_\sigma} |s\rangle \langle s| \otimes W_{\hat{\mathbb{A}}_s} \right) (U_{\text{prep}} \otimes I), \quad (39)$$

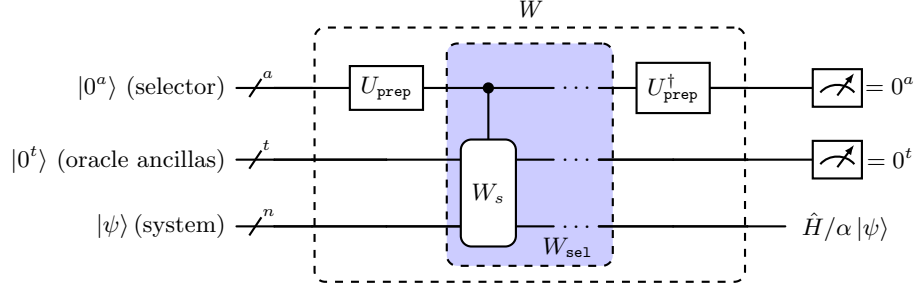


FIG. 3. Binary-multiplexed PREP-SELECT-PREP[†] circuit realizing the unitary W . The SELECT stage implements the controlled table $W_{\text{sel}} = \sum_s |s\rangle \langle s| \otimes (e^{i\phi_s} W_s)$, where phases ϕ_s absorb coefficient signs/phases. The blue dashed fan-out applies W_s when the selector encodes $|s\rangle$. The workspace register has fixed width $t = \max_s t_s$ (including any adaptor-internal index/flag/signal qubits); adaptors with smaller workspace act trivially on unused ancillas. The t oracle ancillas required by a single W_s are reused across branches and projected to $|0^t\rangle$.

with

$$U_{\text{prep}}(\mathcal{M}^{(m)}) |0^{a'}\rangle = \frac{1}{\sqrt{\bar{\alpha}'}} \left(\sum_{s \in \mathcal{M}^{(m)}} \sqrt{2|\omega_s| \alpha_s} |s\rangle + \sqrt{\bar{\alpha}' - \sum_{s \in \mathcal{M}^{(m)}} 2|\omega_s| \alpha_s} |0\rangle \right), \quad (40)$$

where $a' = \lceil \log_2 \ell_\sigma \rceil$ and the additional label $|0\rangle$ is a *null branch* whose SELECT action is the identity. Also, here we fix a *global* normalization

$$\bar{\alpha}' = \sum_{s=1}^{\ell_\sigma} 2|\omega_s| \alpha_s \quad (41)$$

that is independent of the mask (worst-case over the full compiled term list). Because $\omega_s \in \mathbb{R}$ may have either sign, we implement $\text{sgn}(\omega_s)$ as a fixed phase in the corresponding SELECT branch (equivalently, as a π phase on $|s\rangle$ in the PREP state), so that the effective linear combination reproduces $\sum_s \omega_s \hat{A}_s$ rather than $\sum_s |\omega_s| \hat{A}_s$. Projecting the ancillas yields

$$\|(\langle 0^{a'+1}| \otimes I) U_{\hat{\sigma}} (|0^{a'+1}\rangle \otimes I) - \hat{\sigma}/\bar{\alpha}'\| \leq \epsilon', \quad (42)$$

with the block-encoding error

$$\epsilon' = \frac{4}{\bar{\alpha}'} \sum_s |\omega_s| \alpha_s \epsilon_s. \quad (43)$$

b. Exponentiation via a single QSP ladder [50, 51]. Given the block encoding $U_{\hat{\sigma}}$, we apply quantum signal processing to approximate the matrix function $f(x) = e^{-i\bar{\alpha}'x}$ on $[-1, 1]$. This yields

$$\|(\langle 0| \otimes I) Q(\phi, U_{\hat{\sigma}}) (|0\rangle \otimes I) - e^{\hat{\sigma}}\| \leq \epsilon''(\epsilon', \epsilon), \quad (44)$$

where ϵ'' depends linearly on ϵ' (the block-encoding error) and ϵ (the polynomial approximation error). The required polynomial degree scales as

$$d = \mathcal{O}(\bar{\alpha}' + \log(1/\epsilon)), \quad (45)$$

with all dependence on the coefficients ω_s absorbed into $\bar{\alpha}'$.

c. Circuit depth and mask dependence. The QSP circuit uses one signal qubit and d controlled applications of $U_{\hat{\sigma}}$. Since $\text{depth}(U_{\hat{\sigma}}) = \mathcal{O}(\text{depth}(U_{\text{prep}}) + \ell_\sigma \text{depth}(c-U_{\hat{A}_s}))$, the overall depth scales as

$$\text{depth}(e^{\hat{\sigma}}) = \mathcal{O}(d \text{depth}(U_{\hat{\sigma}})). \quad (46)$$

A classical mask is incorporated by reparameterizing only $U_{\text{prep}}(\mathcal{M}^{(m)})$ while keeping the global normalization $\bar{\alpha}'$ fixed via the null branch. Consequently the SELECT table, ancilla wiring, and the QSP phase list (constructed for $\bar{\alpha}'$) are reused verbatim for every mask.

Details of the QSP polynomial construction and error analysis are provided in Appendix C.

C. Similarity-sandwiched effective Hamiltonian

With individual rank-one operators and their exponentials now in hand, we turn to encoding similarity-transformed Hamiltonians with respect to an anti-Hermitian generator and to projecting the result onto a reduced model space. In practice, after constructing the full exponential, we often wish to restrict the similarity transformation to only a subset of excitation operators—for example, to study active spaces of increasing size or to perform incremental downfolding. We capture such choices using a *mask*: a classical bit string that specifies which

rank-one terms are retained. The following paragraphs show how this mask is injected and how it propagates through the block-encoding pipeline.

a. Classical mask. Throughout the remainder of this section we assume that, at run time, a *mask*

$$\mathcal{M}^{(m)} \subset \{1, \dots, \ell_\sigma\} \quad (47)$$

is supplied, where the superscript (m) labels the m -th choice of mask. The mask is a purely classical object that selects which rank-one generators $\{\hat{\mathbb{A}}_s\}$ (already block-encoded in Sec. IV B) are retained. Because the mask is classical, it incurs no coherence or ancilla overhead. Diagnostics for when the fixed rank-one algebraic structure remains stable, together with MP2-guided heuristics for constructing such masks in practice, are provided in Appendix E.

The truncated anti-Hermitian generator is therefore

$$\hat{\sigma}^{(m)} = \sum_{s \in \mathcal{M}^{(m)}} -i\omega_s \hat{\mathbb{A}}_s, \quad \hat{\mathbb{A}}_s = i(\hat{L}_s - \hat{L}_s^\dagger), \quad (48)$$

and the corresponding block encoding $U_{\hat{\sigma}}^{(m)}$ of $\exp(\hat{\sigma}^{(m)})$ is obtained by modifying only the state-preparation amplitudes in the selector register,

$$U_{\text{prep}}(\mathcal{M}^{(m)}) |0^{a'}\rangle = |\chi^{(m)}\rangle. \quad (49)$$

All other components of the circuit—including the SELECT table, ancilla registers, and QSP phase list—remain unchanged.

b. One-shot similarity sandwich. Given the binary-multiplexed Hamiltonian block encoding W from Theorem 1, we form the similarity-sandwiched unitary

$$W_{\text{eff}}^{(m)} = U_{\hat{\sigma}}^{(m)\dagger} W U_{\hat{\sigma}}^{(m)}, \quad (50)$$

which is unitary on the joint ancilla–system space and inherits the same normalization factor α as W . Projecting all ancillas onto $|0_{\text{anc}}\rangle$ yields the normalized system-space block $(\langle 0_{\text{anc}}| \otimes I) W_{\text{eff}}^{(m)} (|0_{\text{anc}}\rangle \otimes I)$. We then define a user-specified *model-space projector* $P^{(m)}$ whose range is a chosen subspace $\mathcal{H}_{\text{mod}}^{(m)} := \text{Ran}(P^{(m)}) \subseteq \mathcal{H}_{N_e}$ (e.g., an active-space determinant set or a truncated excitation manifold) consistent with the mask $\mathcal{M}^{(m)}$. In COMPOSER, $P^{(m)}$ is not assumed to be implemented as a coherent projector inside the oracle; rather, it specifies the subspace on which we represent the effective Hamiltonian (e.g., via matrix elements in a subspace-diagonalization routine). Accordingly, the encoded effective Hamiltonian guarantee is a bound on the *restricted block*:

$$\left\| P^{(m)} \left[(\langle 0_{\text{anc}}| \otimes I) W_{\text{eff}}^{(m)} (|0_{\text{anc}}\rangle \otimes I) - \hat{H}_{\text{eff}}^{(m)} / \alpha \right] P^{(m)} \right\| \leq \epsilon''' . \quad (51)$$

where $P^{(m)}$ is defined as a user-specified model-space projector (e.g., an active-space determinant set or a truncated excitation manifold) that is consistent with the chosen mask $\mathcal{M}^{(m)}$. Equivalently, for all $|\psi\rangle, |\phi\rangle \in \mathcal{H}_{\text{mod}}^{(m)}$, the matrix element error satisfies

$$|\langle \phi | (\langle 0_{\text{anc}}| W_{\text{eff}}^{(m)} |0_{\text{anc}}\rangle - \hat{H}_{\text{eff}}^{(m)} / \alpha) | \psi \rangle| \leq \epsilon''' . \quad (52)$$

Here, the effective Hamiltonian is

$$\hat{H}_{\text{eff}}^{(m)} = P^{(m)} e^{-\hat{\sigma}^{(m)}} \hat{H} e^{\hat{\sigma}^{(m)}} P^{(m)}. \quad (53)$$

The total block-encoding error obeys

$$\epsilon''' = 2\epsilon'' + \epsilon, \quad (54)$$

where ϵ'' is the error from the QSP approximation [Eq. (44)] and ϵ is the Hamiltonian block-encoding error from Theorem 1. The factor of two arises from the two appearances of $U_{\hat{\sigma}}^{(m)}$ in the similarity sandwich. The error bound accumulates additively (up

to constant factors independent of system size) with the number of logical composition layers (LCU, QSP, and the similarity sandwich), while remaining independent of the internal gate depth of each block encoding.

c. Relation to Schrieffer–Wolff (SW) effective Hamiltonians. If P projects onto a target model space and $Q = I - P$, an SW transformation chooses an anti-Hermitian $\hat{\sigma}$ such that the transformed Hamiltonian is (approximately) block diagonal, $Q e^{-\hat{\sigma}} H e^{\hat{\sigma}} P \approx 0$, yielding an effective model-space Hamiltonian $H_{\text{eff}} = P e^{-\hat{\sigma}} H e^{\hat{\sigma}} P$. In COMPOSER, we do not prescribe how $\hat{\sigma}$ is obtained (perturbative SW, variational fitting, or flow-based updates); instead we provide a compile-once oracle that evaluates the masked sandwich $P^{(m)} e^{-\hat{\sigma}^{(m)}} H e^{\hat{\sigma}^{(m)}} P^{(m)}$ while keeping the two-qubit topology fixed. The classical mask $\mathcal{M}^{(m)}$ may be interpreted as selecting which couplings are actively eliminated (or retained) in a truncated

SW generator, enabling systematic model-space refinement without circuit recompilation.

Remark. If one wishes to enforce model-space restriction coherently inside the oracle (rather than treating $P^{(m)}$ as a specification of which matrix elements are queried), one may introduce an additional membership oracle for $\mathcal{H}_{\text{mod}}^{(m)}$ and use it to (i) flag leakage out of the model space or (ii) postselect/amplify within $\mathcal{H}_{\text{mod}}^{(m)}$. Such enforcement is application dependent and is outside the scope of the compile-once block-encoding construction presented here.

d. Mask updates require only re-dialing angles. Switching from $\mathcal{M}^{(m)}$ to a new mask $\mathcal{M}^{(m')}$ leaves the selector register, the SELECT table W_{sel} , the QSP phase list $\{\phi_k\}$, and all ancilla wiring untouched. Only the rotation angles in the deterministic state-preparation ladder that prepares $|\chi^{(m')}\rangle$ are updated. Consequently, the circuit topology is compiled once and reused verbatim across all mask choices. The overall masked similarity-sandwich workflow is sketched in Figure 4.

D. Resource analysis and practical advantages

The block encoding of the effective Hamiltonian constructed above involves two independent linear combinations:

- a *masked generator* $\hat{\sigma}^{(m)} = \sum_{s \in \mathcal{M}^{(m)}} -i\omega_s \hat{A}_s$ containing ℓ_σ rank-one terms; and
- the physical Hamiltonian $\hat{H} = \sum_{s=1}^{\ell_H} \Omega_s \hat{L}_s$, factorized into ℓ_H rank-one ladders.

We keep these symbols distinct in the resource estimates below.

Gate counts. The selector state-preparation ladder $U_{\text{prep}}(\mathcal{M}^{(m)})$ is implemented using controlled single-qubit rotations and CNOT gates. Its depth scales as $\mathcal{O}(\ell_\sigma)$, arising solely from the number of retained labels.

To keep the depth expressions uniform across ladder types, we define the selector-controlled two-qubit depth of a single adaptor branch by its ladder class:

1. $D^{(I)}(n) := \text{depth}(c-W_s)$ for bilinear ladders (Lemma 1);
2. $D^{(II)}(n, R_\mu) := \text{depth}(c-W_\mu)$ for Cholesky-channel ladders (Lemma 2).

For pair-excitation ladders, we denote the corresponding selector-controlled depth by

$$D^{(II)}(n; \mathcal{G}),$$

which depends on the hardware connectivity graph \mathcal{G} through the routing/scheduling of the four-qubit pair-Givens. Each rank-one adaptor branch acts on the same n -qubit system register and has selector-controlled depth $D^{(I)}(n) = \mathcal{O}(n)$ for bilinear ladders (Lemma 1), $D^{(II)}(n, R_\mu) = \mathcal{O}(n + R_\mu)$ for diagonalized Cholesky-channel ladders (Lemma 2), and $D^{(II)}(n; \mathcal{G})$ for pair-excitation ladders. In particular, Appendix A 3 (Table V) shows that $D^{(II)}(n; \mathcal{G})$ scales as $\mathcal{O}(n^2)$ on linear/heavy-hex connectivity and as $\mathcal{O}(n)$ on 2D grid and all-to-all connectivity under standard scheduling assumptions. Because the selector-controlled adaptors are mutually exclusive, the total depth of the generator SELECT stage scales as

$$\begin{aligned} \text{depth}(W_{\text{sel}}(\sigma)) &= \mathcal{O}\left(\sum_{s=1}^{\ell_\sigma} \text{depth}(c-W_{\hat{A}_s})\right) \\ &= \mathcal{O}(\ell_\sigma D_\sigma^{\max}), \end{aligned} \quad (55)$$

where $D_\sigma^{\max} := \max_{s \in \{1, \dots, \ell_\sigma\}} \text{depth}(c-W_{\hat{A}_s})$. For generators dominated by pair-excitation ladders, $D_\sigma^{\max} \approx D^{(II)}(n; \mathcal{G})$, whereas if only bilinear ladders are used then $D_\sigma^{\max} = D^{(I)}(n) = \mathcal{O}(n)$.

For the Hamiltonian block encoding, we use the same multiplexing construction with $\ell_{\hat{H}} \propto n$ rank-one terms arising from the nested factorization. This yields

$$\text{depth}(W_{\text{sel}}(\hat{H})) = \mathcal{O}\left(\sum_{s=1}^{\ell_H} \text{depth}(c-W_s)\right), \quad (56)$$

independent of the generator mask. In the nested-factorized Hamiltonian of Eq. (13), Eq. (56) decomposes into a bilinear part (one-electron modes) and a quadratic-channel part (Cholesky channels), giving a representative scaling

$$\mathcal{O}\left(R_1 D^{(I)}(n) + \sum_{\mu=1}^K D^{(III)}(n, R_\mu)\right). \quad (57)$$

Applying quantum signal processing with polynomial degree d , the full similarity-sandwiched oracle therefore has depth

$$\begin{aligned} \text{depth}(W_{\text{eff}}^{(m)}) &= \mathcal{O}\left(d \text{depth}(U_{\hat{\sigma}}^{(m)}) + \text{depth}(W)\right) \\ &= \mathcal{O}\left(d \ell_\sigma D_\sigma^{\max} + \text{depth}(W_{\text{sel}}(\hat{H}))\right), \end{aligned} \quad (58)$$

Here the $d \ell_\sigma D_\sigma^{\max}$ contribution arises exclusively from the QSP-controlled applications of the generator block encoding $U_{\hat{\sigma}}$, while the n^2 term originates from the Hamiltonian SELECT stage and is not multiplied by the QSP degree. In particular, the Hamiltonian block encoding is invoked only once inside the similarity sandwich.

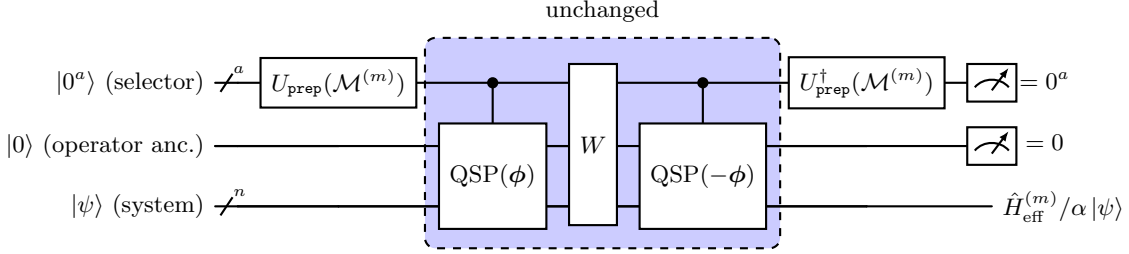


FIG. 4. Compile-once circuit for the similarity-sandwiched effective Hamiltonian. Changing the classical mask $\mathcal{M}^{(m)}$ only redials the rotation angles in $U_{\text{prep}}(\mathcal{M}^{(m)})$; every other gate, ancilla, and QSP phase is reused verbatim for every *mask*.

Ancilla budget. The generator and Hamiltonian linear combinations require selector registers of widths \mathbf{a}_σ and \mathbf{a}_H , respectively. Because these ladders are executed sequentially and the selector register is reset between them, a single physical register of width $\mathbf{a} = \max(\mathbf{a}_\sigma, \mathbf{a}_H)$ suffices. Including adaptor-internal ancillas, the total ancilla width is $\mathbf{a} + t$, where $\mathbf{a} = \max(\mathbf{a}_\sigma, \mathbf{a}_H)$ is the selector width and t is the maximum number of oracle ancillas required by any selected adaptor (e.g., $t = 1$ for bilinear dyads, and $t = \mathbf{a}_I + 2$ for the diagonalized Cholesky-channel adaptor in Lemma 2).

The architectural implications of this scaling—namely, freezing the logical two-qubit topology and streaming only parametric updates—are discussed in detail in Sec. V.

Quantitative payoff: what is avoided under instance updates. Let ℓ_H^{pool} and $\ell_\sigma^{\text{pool}}$ denote the sizes of the *compiled* rank-one term pools for \hat{H} and $\hat{\sigma}$, chosen large enough to cover a target family of instances (e.g., a geometry scan or active-space growth), and let $\ell_\sigma = |\mathcal{M}^{(m)}|$ denote the *active* masked generator size at a particular update. A conventional instance-specific pipeline typically regenerates the term list (or its data-access structure), rebuilds the corresponding multiplexing and routing layers, and re-runs hardware mapping/routing whenever coefficients, truncations, or active spaces change. In COMPOSER, the two-qubit fabric implementing the selector-controlled adaptors and routing is compiled once for $(\ell_H^{\text{pool}}, \ell_\sigma^{\text{pool}})$; a geometry or mask update only *dials* new single-qubit angles (PREP amplitudes and local ladder phases) and streams new classical coefficients/masks. A concrete proxy is the number of two-qubit layers whose placement/routing is compiled once: from Table II, the logical two-qubit depth of one masked similarity-sandwiched oracle scales as $\mathcal{O}(dn \ell_\sigma^{\text{pool}} + n^2)$ and is unchanged across updates, whereas the per-instance compilation cost of an instance-specific build scales with this entire two-qubit fabric [81, 82]. Table III summarizes which objects must be regenerated in a

conventional pipeline versus COMPOSER.

V. ARCHITECTURE, AND COMPILE-ONCE PHILOSOPHY OF COMPOSER

Having established the operator factorizations, adaptor constructions, and resource scalings, we now elevate the discussion to the architectural level. The nested factorizations of \hat{H} and $\hat{\sigma}$ compress both the Hamiltonian and similarity generator into linearly scaling collections of rank-one operators. Each rank-one ladder \hat{L}_s is converted into a deterministic block encoding whose selector-controlled depth depends on its ladder class: $\mathcal{O}(n)$ for bilinear ladders, $\mathcal{O}(n + R_\mu)$ for diagonalized Cholesky-channel ladders, and $D^{(II)}(n; \mathcal{G})$ for pair-excitation ladders, where the latter is connectivity dependent (Appendix A3). These ladders are assembled within a fixed PREP-SELECT-PREP[†] skeleton that defines a reusable two-qubit circuit fabric (Figure 4).

The central design principle of COMPOSER is to disentangle circuit *topology* from numerical *data*. Topology comprises the selector cascade, adaptor layout, and QSP scaffold; data comprises the coefficients and rotation angles that vary with geometry, active space, or mask choice. By freezing the selector-controlled two-qubit structure and allowing only parametric single-qubit updates, COMPOSER shifts adaptation cost from structural recompilation to classical parameter streaming. Importantly, QSP overhead is confined to exponentiation of masked generators; the Hamiltonian block encoding itself remains a single multiplexed layer whose depth is independent of the QSP degree. Figure 4 summarizes the resulting two-phase workflow in a way that separates the one-time compilation work from the per-instance parameter updates (see also Algorithm 1 in Appendix D).

a. Adaptor abstraction. Each rank-one operator is associated with a fixed-topology adaptor that implements its normalized block encoding. Adap-

TABLE II. Logical-level resource scaling for one masked similarity-sandwiched oracle. Depth counts two-qubit layers; single-qubit rotations are treated as depth-1.

Circuit block	System qubits	Ancillas	Depth
Adaptor (bilinear dyad)	n	1 (signal)	$\mathcal{O}(n)$
Adaptor (pair-excitation ladder)	n	1 (signal)	$D^{(II)}(n; \mathcal{G})$ (see Table V)
Adaptor (Cholesky channel)	n	$\mathbf{a}_I + 2$	$\mathcal{O}(n + R_\mu)$
Hamiltonian SELECT	n	$\mathbf{a}_H = \lceil \log_2 \ell_H \rceil$	$\mathcal{O}(n^2)$
Generator SELECT	n	$\mathbf{a}_\sigma = \lceil \log_2 \ell_\sigma \rceil$	$\mathcal{O}(\ell_\sigma D_\sigma^{max})$
PREP amplitude ladder	–	$\max(\mathbf{a}_\sigma, \mathbf{a}_H)$	$\mathcal{O}(\ell_\sigma)$
Two QSP ladders	n	shared signal qubit	$\mathcal{O}(d\ell_\sigma D_\sigma^{max})$
Total	n	$\mathbf{a} + t$	$\mathcal{O}(d\ell_\sigma D_\sigma^{max} + \text{depth}(W_{\text{sel}}(\hat{H})))$

TABLE III. What must be regenerated under instance updates (geometry/mask/truncation) in a conventional instance-specific pipeline versus COMPOSER. “Regenerate” indicates structural recompilation/remapping/rerouting of two-qubit layers; “dial” indicates updating classical coefficients and single-qubit rotation angles while reusing the same two-qubit fabric.

Artifact under updates	Conventional build	COMPOSER
Term list / truncation pattern	regenerate	fixed pool + classical mask
Data-loading for coefficients	regenerate	dial for the same topology
SELECT multiplexer and two-qubit routing	regenerate	compiled once

tors are tagged by binary addresses and embedded in an invariant selector tree determined solely by the total number of rank-one terms. Changes in coefficients or truncation masks modify only PREP amplitudes and local phases; the underlying two-qubit connectivity graph remains unchanged.

b. Compile-once execution model. COMPOSER generates the logical two-qubit schedule of this architecture once [81–83]. Subsequent instance updates—geometry sweeps, active-space growth, or mask refinement—stream new single-qubit angles to the same fixed graph. If a subset of rank-one terms is disabled by a classical mask, the corresponding adaptors are bypassed without altering circuit structure. Here “compile-once” refers specifically to invariance of the logical two-qubit topology; hardware calibration and fault-tolerant synthesis layers remain orthogonal [94–96].

c. Subspace diagonalization workloads (GCIM/QSE/NOQE) as a natural dial-many target. The compile-once premise is particularly well aligned with subspace diagonalization workflows in which one repeatedly evaluates *families* of closely related state-preparation circuits to build projected matrices H and S . In QSE/NOQE/GCIM-style solvers, basis states are often generated by exponentiating a small set of anti-Hermitian operators drawn from a common pool, and the working subspace is expanded by activating additional generators or adjusting their scalar weights [28–32]. In COMPOSER such updates correspond precisely to re-dialing the PREP angles

and classical masks/selectors while leaving the two-qubit fabric (selector cascade, adaptor layout, and QSP scaffold) unchanged. This enables a unified compiled circuit template for both expectation-value measurements and overlap measurements between different masked basis states, even as the subspace is adaptively enlarged.

d. Fault-tolerant angle synthesis (what compile-once does and does not buy). The compile-once promise of COMPOSER is about *logical topology* (the two-qubit connectivity pattern and routing plan). In a fault-tolerant setting, this logical circuit must still be lowered to a discrete gate set (e.g., Clifford+ T), and the cost of synthesizing the updated single-qubit rotations can dominate when high precision is required. Thus, compile-once should be read as *eliminating topology recompilation* (remapping/rerouting/re-optimizing the two-qubit fabric) across instance updates, while leaving rotation-synthesis overhead as an orthogonal, accuracy-controlled layer [94–96]. In practice, the rotation-synthesis tolerance can be incorporated into the same error budget that already allocates block-encoding and QSP approximation errors (Appendix D).

e. One canonical closed-loop workflow for updating $\hat{\sigma}$ and masks. A typical usage pattern is: (i) choose an orbital pool/basis and compile the circuit skeleton once (Algorithm 1); (ii) for each geometry or active-space choice, compute integral-derived low-rank factors for \hat{H} and obtain an inexpensive proxy for the similarity generator (e.g., MP2- or

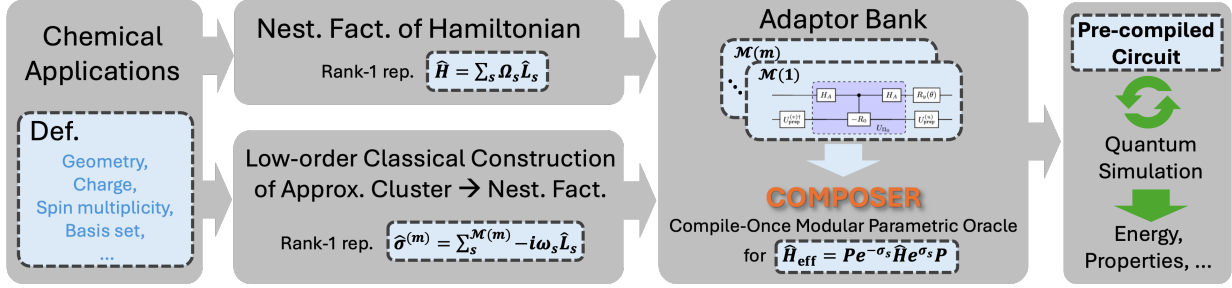


FIG. 5. Schematic workflow for quantum simulation using COMPOSER. The two-qubit circuit topology is fixed in a one-time synthesis pass; subsequent updates to molecular geometry, active space, or truncation mask re-dial only single-qubit rotations.

low-order SW-seeded amplitudes), then screen to define a mask $\mathcal{M}^{(m)}$; (iii) run the fixed oracle to evaluate energies/observables in the current model space; and (iv) refine by expanding the mask/active space or updating the generator parameters, while reusing the same compiled two-qubit fabric. Across this loop, the selector tree, adaptor wiring, and QSP scaffold remain fixed; only the classical coefficients/masks and the corresponding single-qubit angles are updated.

f. Error budget. The total tolerance ϵ_{tot} decomposes into factorization, block-encoding, multiplexing, and QSP contributions. Separately, any error due to the choice of encoded operators (e.g., a CCSD-seeded truncated generator or a particular mask) is a modeling/initialization consideration and can be improved by refining the encoded data without changing the compiled two-qubit topology. This separation exposes independent control knobs for depth–accuracy tradeoffs without modifying the frozen topology (Appendix D).

COMPOSER therefore reorganizes standard block-encoding primitives into a topology-invariant execution paradigm. Rather than altering asymptotic query complexity, it enforces structural reuse across families of closely related operators, enabling predictable resource scaling in adaptive quantum workflows.

VI. RELATION TO LOCAL JASTROW ANSATZ, TENSOR NETWORKS, AND CANONICAL TRANSFORMATIONS

The rank-one quadratic occupation operators arising from the nested factorization in COMPOSER bear a close relationship to both *local Jastrow* correlation factors and *tensor-network* operator representations. These connections provide additional physical and structural intuition for the resulting block-encoding

architecture, but are not required for its construction.

a. Connection to the local Jastrow ansatz. A (generally *non-unitary*) Jastrow correlation factor in lattice/second-quantized form is often written as [92]

$$e^{\sum_{p<q} u_{pq} n_p n_q}, \quad (59)$$

where $n_p = a_p^\dagger a_p$ is the occupation operator of orbital p . For real u_{pq} , this operator is diagonal in the occupation basis and preserves particle number, but it *reweights* configuration amplitudes rather than applying phases. A *unitary* (phase-imprinting) variant frequently used in quantum-circuit contexts replaces the exponent by $-i \sum_{p<q} \theta_{pq} n_p n_q$, yielding a diagonal unitary that applies configuration-dependent phases [97–99].

In COMPOSER, the projected quadratic rank-one operators [Eq. (13)] take a closely related form: they are diagonal *in a channel-dependent rotated orbital basis* (e.g., the eigenbasis of each Cholesky/DF channel), and preserve particle number, but their coefficients are not free variational parameters—they emerge directly from the electronic-structure data and chosen factorization thresholds. In the original computational basis, these operators become diagonal only after conjugation by the corresponding single-particle rotation (implemented by the same deterministic ladder/Givens primitives used elsewhere in COMPOSER). If one chooses to exponentiate such diagonal quadratic forms as part of a similarity generator (e.g., unitary cluster-Jastrow layers), they generate Jastrow-like correlation patterns with *data-driven* coefficients [97, 98].

b. Connection to tensor networks. The nested factorization of \hat{H} and $\hat{\sigma}$ produces sums of outer products of low-dimensional coefficient vectors, which is closely related to the low-rank decompositions used to obtain compact matrix product operator (MPO) forms [100–106]. From this perspective:

- the selector register in COMPOSER plays the role of a virtual (bond) index that labels which low-rank operator branch is active;
- the overall PREP-SELECT-PREP[†] construction is naturally interpreted as a *star-shaped* (LCU/CP-like) operator tensor network rather than a strictly site-local MPO chain;
- each rank-one adaptor corresponds to a structured operator tensor associated with one selector value; and
- the fixed PREP-SELECT-PREP[†] skeleton defines the network connectivity, while single-qubit rotation angles supply the tensor entries.

This viewpoint highlights that COMPOSER can be regarded as a hardware-native, fixed-topology tensor-network *execution* skeleton whose numerical content is updated efficiently via classical streaming of angles rather than circuit recompilation.

c. Connection to Schrieffer–Wolff and canonical transformations. Schrieffer–Wolff (SW)-type downfolding and related canonical-transformation formalisms can be viewed as generating effective interactions (after similarity transformation and projection) that are often dominated by density–density and other structured low-body terms in an appropriate basis [33, 34, 38]. The Jastrow-like (diagonal) and tensor-network-like (low-rank) perspectives above therefore provide an intuitive bridge: COMPOSER supplies a compile-once block-encoding fabric that can repeatedly *update* such effective couplings across masks/model spaces without recompiling two-qubit routing, aligning naturally with iterative SW-style workflows.

Conceptually, COMPOSER unifies (i) diagonal, number-conserving quadratic structure reminiscent of Jastrow correlators; (ii) structured low-rank decompositions characteristic of tensor networks; and (iii) a depth-optimized, compile-once quantum circuit topology. This synthesis enables structured effective interactions to be encoded within a tensor-network-inspired operator skeleton while retaining the flexibility and resource efficiency of the mask-aware execution model.

VII. NUMERICAL DEMONSTRATION

The numerical tests reported in this section use a small benchmark set of closed-shell molecules spanning increasing system size and bonding complexity: H₂, H₂O, NH₃, CH₄, H₂CO, C₂H₄, CH₃OH, C₂H₆, and C₆H₆. These systems include diatomic, triatomic, and polyatomic species with single, double, and aromatic bonding motifs, and involve C,

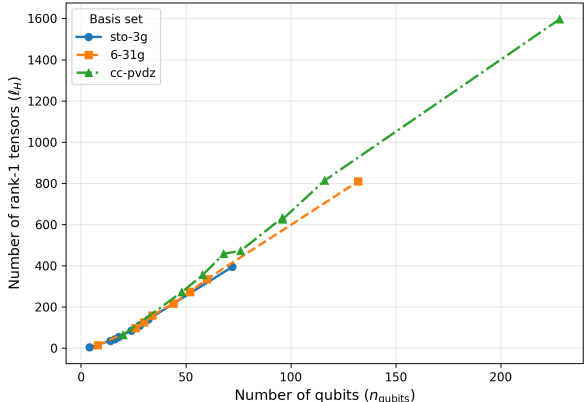


FIG. 6. Scaling of the total number of rank-1 tensors l_H required for Hamiltonian block encoding as a function of the number of qubits n_{qubits} . Results are shown for three commonly used Gaussian basis sets: STO-3G, 6-31G, and cc-pVDZ. Each data point corresponds to a molecular system included in the benchmark set, with n_{qubits} determined by the number of spin orbitals in the chosen basis. The approximately linear trend over the tested range indicates empirically quasi-linear growth of the rank-1 ladder pool with system size, while the vertical offsets reflect the increased two-electron integral complexity of larger basis sets. All data use a fixed Cholesky threshold $\tau_{\text{chol}} = 10^{-8}$ (and channel eigenvalue cutoff $\tau_{\text{eig}} = 10^{-4}$), so that the observed quasi-linear growth reflects empirical scaling of the required Cholesky-channel count K with system size for chemically relevant tolerances.

H, O, and N atoms. All geometries were fixed at standard equilibrium structures. For each molecule, calculations were performed in the STO-3G, 6-31G, and cc-pVDZ basis sets.

Unless stated otherwise, all calculations use restricted Hartree–Fock canonical orbitals and a fixed electron number with no symmetry breaking. Two-electron integrals are factorized via pivoted Cholesky with threshold $\tau_{\text{chol}} = 10^{-8}$, which determines the number of Cholesky channels K and hence the rank-one Hamiltonian pool size l_H [Eq. (17)]. For each channel, eigenmodes with $|\lambda_{\xi}^{(\mu)}| / \max_{\xi} |\lambda_{\xi}^{(\mu)}| < \tau_{\text{eig}} = 10^{-4}$ are discarded, defining R_{μ} . MP2 amplitudes follow Møller–Plesset second-order perturbation theory, and CCSD amplitudes are obtained from converged coupled-cluster singles and doubles equations with energy residual tolerance 10^{-6} a.u.

We present numerical evidence that the *structural conditions required for topology-invariant compilation* are satisfied in representative molecular workflows. Specifically, we validate (i) that the nested Hamiltonian factorization yields a rank-one ladder pool whose size grows mildly with system size (so

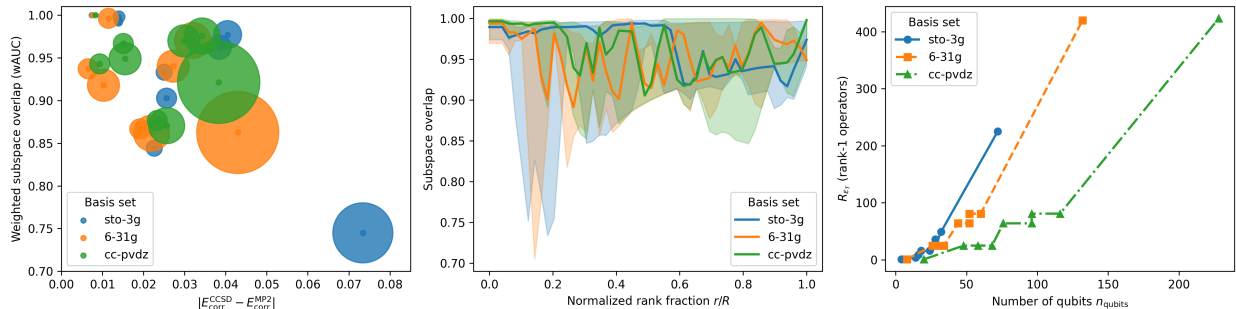


FIG. 7. Cross-molecular validation of MP2-derived rank-1 operator subspaces against CCSD across multiple basis sets. (a) Weighted average subspace overlap (wAUC) between MP2- and CCSD-derived rank-1 spaces for each molecule and basis set (STO-3G, 6-31G, and cc-pVDZ), plotted against the correlation-energy discrepancy $|E_{\text{corr}}^{\text{CCSD}} - E_{\text{corr}}^{\text{MP2}}|$. Marker size encodes the number of retained rank-1 operators R_ϵ , defined by a global relative singular-value screening criterion $s_k/s_1 \geq \epsilon_s$ applied to the CCSD T_2 spectrum. (b) Median MP2–CCSD subspace overlap as a function of normalized rank fraction r/R , with shaded regions indicating the interquartile range across all molecules for each basis set. (c) Scaling of the number of retained rank-1 operators R_ϵ with the number of qubits n_{qubits} , illustrating the growth of the dominant T_2 operator manifold with system size and basis-set quality.

the SELECT fabric can be fixed), and (ii) that low-rank excitation subspaces are stable under inexpensive classical proxies (so *mask updates* can be realized by re-dialing PREP amplitudes without restructuring the circuit). Accordingly, the goal of this section is *not* to benchmark chemical energies or fault-tolerant Toffoli counts, but to support the architectural premise of Figure 1: across families of closely related instances (basis choice, molecule size, and masking), the logical two-qubit topology can remain unchanged while instance dependence enters only through streamed single-qubit parameters.

a. Scaling of rank-one Hamiltonian factorizations. Figure 6 shows the total number of rank-one tensors ℓ_H required to represent the electronic Hamiltonian as a function of the number of qubits n_{qubits} , for three commonly used Gaussian basis sets (STO-3G, 6-31G, and cc-pVDZ). Here ℓ_H denotes the number of *rank-one adaptor branches* in the Hamiltonian LCU, i.e., $\ell_H = R_1 + K$ in Eq. (17), where R_1 is the number of retained one-electron modes (typically $R_1 \approx n_{\text{qubits}}$ in the absence of additional truncation) and K is the number of Cholesky channels at threshold τ_{chol} . Thus, the nontrivial scaling signal is primarily the quasi-linear growth of K for fixed τ_{chol} . Each data point corresponds to a molecular system included in the benchmark set, with n_{qubits} determined by the number of spin orbitals in the chosen basis.

Across all basis sets, ℓ_H exhibits empirically quasi-linear growth over the tested molecular range, with basis-set-dependent slopes. Since the selector width is $\mathbf{a}_H = \lceil \log_2 \ell_H \rceil$, this implies only logarithmic growth in the selector register even as the ladder pool expands. As a result, a fixed

PREP–SELECT–PREP[†] multiplexing topology can be chosen once and reused across increasing molecular complexity, satisfying a central structural requirement of the compile-once execution model.

b. Instance-update invariance under geometry scans (compile-once stress test). We performed a short geometry scan for H₂O by scaling the equilibrium H–O bond length R_e by factors 0.5, 1.0, 1.5, and 2.0 and recomputing the nested Hamiltonian factorization at each geometry. Table IV reports the Cholesky-channel count K and the resulting Hamiltonian ladder count $\ell_H = R_1 + K$ across three basis sets. Over the full scan window, ℓ_H varies mildly (STO-3G: constant at 35; 6-31G: 94–97; cc-pVDZ: 239–272), so the selector width can be fixed once as $\mathbf{a}_H = \lceil \log_2 \ell_H^{\text{max}} \rceil$ without changing any two-qubit multiplexing/routing structure. Geometry dependence is absorbed entirely into updated single-qubit angles in PREP and local ladder phases, consistent with the compile-once premise. In particular, for each basis we can fix $\mathbf{a}_H = \lceil \log_2 \ell_H \rceil$ at the maximum value over the scan window and treat all geometry dependence as streamed updates to the PREP angles.

c. Stability of low-rank excitation subspaces. Figure 7 examines the robustness of low-rank excitation manifolds derived from inexpensive perturbative calculations. Here the subspace overlap between MP2 and CCSD rank-one manifolds is computed from the top- r left singular subspaces of the reshaped T_2 tensor (pair-virtual \times pair-occupied), using the normalized projector overlap $\text{ov}(r) = \frac{1}{r} \|P_r^{\text{MP2}} P_r^{\text{CCSD}}\|_F^2$ (equivalently, the mean squared cosine of principal angles). Panel (a) shows the weighted average subspace overlap (wAUC) between

TABLE IV. H₂O geometry-scan stress test for topology-invariant compilation. We vary the H–O bond length from $0.5R_e$ to $2.0R_e$ (with R_e the equilibrium bond length) and report the Cholesky-channel count K and total Hamiltonian rank-one ladder count $\ell_H = R_1 + K$ (shown as K/ℓ_H). The compiled selector width can be fixed for each basis as $\alpha_H = \lceil \log_2 \ell_H^{\max} \rceil$ over the scan window.

Basis	$0.5R_e$	$1.0R_e$	$1.5R_e$	$2.0R_e$	ℓ_H^{\max}	$\alpha_H = \lceil \log_2 \ell_H^{\max} \rceil$
sto-3g	28/35	28/35	28/35	28/35	35	6
6-31g	84/97	84/97	84/97	81/94	97	7
cc-pVDZ	232/256	248/272	230/254	215/239	272	9

MP2-derived and CCSD-derived rank-one excitation spaces, plotted against the correlation-energy discrepancy $|E_{\text{corr}}^{\text{CCSD}} - E_{\text{corr}}^{\text{MP2}}|$. Marker size indicates the number of retained rank-one operators R_ϵ selected using a global singular-value threshold. The reported wAUC is a weighted average of $\text{ov}(r)$ over $r \leq R$, with weights chosen to emphasize the leading ranks (see Appendix E for the exact definition). Across the benchmark set, the median wAUC remains 0.85 or higher in all three basis sets, with the lowest-outlier cases occurring for C₆H₆ where MP2 correlation energy employing STO-3G basis set differs most strongly from CCSD.

Despite variations in correlation energy and basis set, the dominant excitation subspaces exhibit consistently high overlap, indicating that MP2 captures the leading algebraic structure of the CCSD excitation manifold. Panel (b) further shows that this agreement persists as a function of normalized rank fraction r/R , with median overlaps remaining close to unity across basis sets. Panel (c) illustrates the growth of the retained rank-one operator count R_ϵ with system size, demonstrating that the dominant excitation space grows systematically but remains a small fraction of the full T_2 manifold.

In SW-type effective Hamiltonian constructions, the generator is chosen to suppress couplings between a model space and its complement, and practical implementations rely on truncating this generator to a structured subset of dominant channels. The observed stability of low-rank T_2 -derived manifolds under MP2 proxies provides numerical support for such truncation/masking heuristics: it suggests that the leading couplings that would enter a low-order SW generator can be identified inexpensively and then updated across related instances (e.g., along a geometry scan) by streaming coefficient changes rather than recompiling the two-qubit fabric.

Collectively, these results justify MP2-guided truncation and masking strategies in COMPOSER: a relatively small number of rank-one operators can capture the dominant excitation subspace across a broad range of molecules and basis sets. Architecturally, this stability underpins mask-aware workflows in which refinement proceeds by updating classical masks and re-dialing PREP amplitudes, while

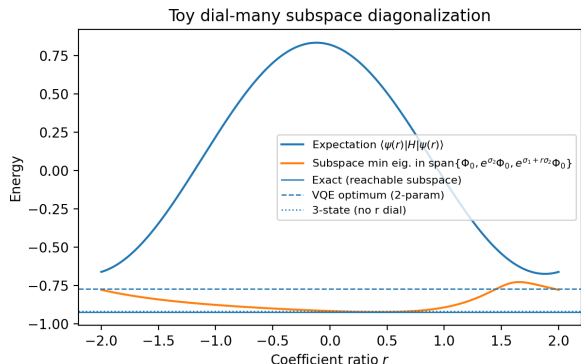


FIG. 8. Toy illustration of a “compile-once, dial-many” non-orthogonal subspace solve aligned with the COMPOSER execution model. A fixed state-preparation topology generates a small non-orthogonal determinant basis from a shared operator pool and supports a continuous generator-coordinate sweep by re-dialing a single classical coefficient.

preserving the underlying multiplexed circuit fabric. See Appendix E for the MP2-guided truncation procedure and stability diagnostics underlying these masking choices. We emphasize that this section supports a different objective than reducing asymptotic query complexity: it supports eliminating *structural recompilation* across instance families by ensuring that the operator representation admits a stable, fixed-topology multiplexed realization. A detailed comparison of logical gate counts or fault-tolerant resource estimates under different masking strategies is deferred to future work.

d. Illustrative end-to-end subspace diagonalization with a continuous generator-coordinate dial. Figure 8 provides a minimal end-to-end illustration of this “compile-once, dial-many” pattern in a non-orthogonal subspace solve. Here, we consider a 4-qubit, 2-electron determinant subspace generated from a reference $|\Phi_0\rangle = |1100\rangle$ by two commuting anti-Hermitian generators ($\hat{\sigma}_1, \hat{\sigma}_2$) implemented as number-conserving Givens rotations on disjoint orbital pairs. A conventional separable product ansatz $|\psi(\theta_1, \theta_2)\rangle = e^{\theta_2 \hat{\sigma}_2} e^{\theta_1 \hat{\sigma}_1} |\Phi_0\rangle$ is expressivity-limited and converges to a higher energy

(here $E_{\text{VQE}} = -0.774$ in arbitrary units), while a small non-orthogonal basis $\{|\Phi_0\rangle, e^{\hat{\sigma}_1}|\Phi_0\rangle, e^{\hat{\sigma}_2}|\Phi_0\rangle\}$ yields a much lower generalized-eigenvalue estimate ($E = -0.918$). Finally, sweeping a continuous generator coordinate r in $e^{\hat{\sigma}_1+r\hat{\sigma}_2}|\Phi_0\rangle$ within the fixed 3-state span $\{|\Phi_0\rangle, e^{\hat{\sigma}_2}|\Phi_0\rangle, e^{\hat{\sigma}_1+r\hat{\sigma}_2}|\Phi_0\rangle\}$ recovers the exact subspace ground energy (here $E_{\text{exact}} = -0.924$) without changing circuit topology, illustrating the “compile-once, dial-many” premise in a subspace-diagonalization setting. From the COMPOSER perspective, both discrete basis updates (activating/deactivating generators via masks) and continuous updates (changing coefficient ratios such as r) correspond to re-dialing PREP angles and classical selector data, while leaving the compiled two-qubit fabric unchanged. We emphasize that the objective here is not to reduce asymptotic query complexity, but to eliminate *structural recompilation* across instance families by ensuring that the operator representation admits a stable, fixed-topology multiplexed realization.

VIII. CONCLUSION AND OUTLOOK

COMPOSER provides a practical bridge from nested low-rank tensor factorizations to hardware-native, mask-aware block encodings for molecular simulation. By fixing the multiplexing topology and encapsulating all instance dependence in single-qubit rotations, it delivers depth-optimal oracles driven by a single QSP ladder, predictable ancilla budgets comprising only selector and signal registers, and zero recompilation overhead across geometry sweeps, active-space growth, and adaptive similarity transformations. These properties are supported by numerical evidence demonstrating near-linear scaling of rank-one Hamiltonian factorizations and robustness of low-rank excitation subspaces, which validate the structural assumptions of the architecture.

Beyond downfolded Hamiltonian simulation, the same mask-aware interface is immediately applicable to non-orthogonal subspace solvers that require repeated evaluation of Hamiltonian and overlap matrix elements in an expanding basis (e.g., QSE/NOQE/GCIM), since basis-state updates can be expressed as mask/parameter updates on a fixed oracle template [28–32]. This offers a concrete end-to-end application in which the compile-once principle directly mitigates the otherwise quadratic growth in distinct compiled circuits as the subspace dimension increases.

Methodologically, deterministic, number-conserving ladders provide a unified implementation of bilinear, pair-excitation, and projected-quadratic rank-one operators, enabling efficient block encod-

ings for both Hamiltonians and anti-Hermitian generators. Practically, the mask-aware “compile-once, dial-later” execution model reduces end-to-end latency, simplifies resource estimation, and decouples adaptive algorithm design from circuit recompilation—features that are particularly attractive for NISQ demonstrations and early fault-tolerant deployments.

We emphasize that the present work is architectural rather than competitive in asymptotic resource counts. Detailed logical Toffoli estimates and fault-tolerant overhead comparisons under specific hardware models are natural next steps, but are orthogonal to the compile-once principle developed here. The numerical results validate the structural premises (low-rank operator growth and excitation-subspace stability) that justify freezing the logical circuit topology, rather than demonstrating an end-to-end runtime advantage over existing simulation frameworks.

Looking ahead, natural extensions of this work include automated hardware-aware scheduling of two-qubit gates for large instances on heavy-hex and grid-based architectures, systematic studies of mask-selection strategies and error-budget allocation, and generalizations beyond electronic structure to lattice models and open-system generators. Angle-selection and refinement (Sec. V and Introduction) remain important directions, including systematic improvements beyond CCSD-seeded doubles via tighter factorizations, expanded operator pools, or hybrid diagnostic-guided updates—without altering the fixed two-qubit topology. More broadly, the connections between projected-quadratic ladders, local Jastrow factors, and tensor-network operator representations suggest a unifying perspective in which fixed-topology, data-driven quantum circuits capture correlation efficiently across a wide range of quantum simulation settings.

ACKNOWLEDGMENTS

B.P. acknowledges the support from the Early Career Research Program by the U.S. Department of Energy, Office of Science, under Grant No. FWP 83466. Y.L. acknowledges the support by the U.S. Department of Energy, Office of Science, Advanced Scientific Computing Research, under contract number DE-SC0025384. K.K. acknowledges the Quantum Algorithms and Architecture for Domain Science Initiative (QuAADS), a Laboratory Directed Research and Development (LDRD) program at PNNL.

Appendix A: Deterministic Ladder Constructions and Hardware Realizations

This appendix collects implementation-level details for the deterministic ladder circuits used in Secs. III A and III B. In the main text we emphasize the existence, fixed topology, and number-conserving nature of these ladders; here we record explicit angle recursions and convenient product decompositions that can be used directly in code generation. Throughout this appendix we use the convention $\prod_{k=1}^m U_k := U_m \cdots U_2 U_1$ (rightmost factor acts first).

1. One-electron ladder: recursion and explicit product form

Fix an ordering $(p_1, p_2, \dots, p_{n-1})$ of non-pivot orbitals (with pivot r). The ladder rotation angles may be chosen recursively. Define tail norms $s_k := \sqrt{|u_r|^2 + \sum_{j \geq k} |u_{p_j}|^2}$ for $k = 1, \dots, n-1$, and set $s_n := |u_r|$. A convenient deterministic choice of ladder angles is then

$$\begin{aligned} \theta_{p_k r} &= \arctan\left(\frac{|u_{p_k}|}{s_{k+1}}\right) \\ &= \arctan\left(\frac{|u_{p_k}|}{\sqrt{|u_r|^2 + \sum_{j > k} |u_{p_j}|^2}}\right), \end{aligned} \quad (\text{A1})$$

equivalently $\sin \theta_{p_k r} = |u_{p_k}|/s_k$ and $\cos \theta_{p_k r} = s_{k+1}/s_k$. so that amplitude is transferred sequentially from $|r\rangle$ to the desired orbitals with correct magnitudes. Residual complex phases are restored by diagonal phase shifts on orbitals; since the overall many-body phase is irrelevant we may fix the gauge so that $u_r \in \mathbb{R}_{\geq 0}$ and apply $R_z^{(p)}(\phi_p)$ with $\phi_p = \arg(u_p)$ for $p \neq r$ (or include $p = r$ as well, which changes only a global phase).

Collecting all operations yields the preparation-form ladder unitary. Define a real-amplitude ladder $V_u := \prod_{k=1}^{n-1} G_{p_k r}(\theta_{p_k r})$ and a diagonal phase operator $D_u := \prod_{p \neq r} R_z^{(p)}(\arg u_p)$. Then the preparation-form ladder may be written compactly as

$$U_{\text{prep}}^{(u)} = D_u V_u X_r, \quad (\text{A2})$$

which satisfies $U_{\text{prep}}^{(u)}|0^n\rangle = |u\rangle$. The inverse is obtained by reversing the gate order and negating all angles.

2. Two-electron ladder: recursion and explicit product form

Fix an ordering of the non-pivot unordered pairs $(p_1, q_1), \dots, (p_m, q_m)$ with $m = \binom{n}{2} - 1$ (pivot pair (r, s)). The ladder angles and phases may be chosen as follows. Define tail norms $s_k := \sqrt{|u_{rs}|^2 + \sum_{j \geq k} |u_{p_j q_j}|^2}$ for $k = 1, \dots, m$, and set $s_{m+1} := |u_{rs}|$. A convenient deterministic choice is

$$\begin{aligned} \theta_k &= \arctan\left(\frac{|u_{p_k q_k}|}{s_{k+1}}\right) \\ &= \arctan\left(\frac{|u_{p_k q_k}|}{\sqrt{|u_{rs}|^2 + \sum_{j > k} |u_{p_j q_j}|^2}}\right), \end{aligned} \quad (\text{A3})$$

equivalently $\sin \theta_k = |u_{p_k q_k}|/s_k$ and $\cos \theta_k = s_{k+1}/s_k$. Here, amplitude and phase are transferred sequentially from the pivot pair to the desired determinants. $\phi_k = \arg(u_{p_k q_k})$ fixes the overall phase so that $u_{rs} \in \mathbb{R}_{\geq 0}$. The corresponding preparation-form ladder is

$$U_{\text{prep}}^{(u)} = \left(\prod_{k=1}^m G_{p_k q_k, rs}(\theta_k, \phi_k) \right) X_r X_s, \quad (\text{A4})$$

which satisfies $U_{\text{prep}}^{(u)}|0^n\rangle = |u\rangle$.

3. Two-Electron Givens-SWAP Networks and Hardware Mapping

This appendix details the routing and scheduling of the two-electron deterministic ladders introduced in Sec. III B, with emphasis on SWAP overheads and connectivity-dependent depth scaling. [70, 71, 81–83]

The two-electron preparation circuit may be expressed directly in terms of the phased pair-Givens blocks from Eq. (32),

$$U_{\text{prep}}^{(u)} = \left(\prod_{k=1}^m G_{p_k q_k, rs}(\theta_k, \phi_k) \right) X_r X_s. \quad (\text{A5})$$

In practice, the phase parameter ϕ_k is realized by a constant-depth pattern of local Z rotations within the fixed four-qubit block implementing $G_{p_k q_k, rs}$, which enables consolidation of many diagonal phases across neighboring blocks. Below we summarize routing strategies that minimize depth under common hardware connectivity assumptions.

a. Minimal SWAP schedule During the ladder execution, the pivot pair (r, s) must remain adjacent.

A single-pivot routing scheme suffices:

$$\begin{aligned} (r, s, q_1, q_2) &\xrightarrow[(r, q_1)]{\text{fSWAP}} (q_1, s, r, q_2) \\ &\xrightarrow[(s, q_2)]{\text{fSWAP}} (q_1, q_2, r, s), \end{aligned} \quad (\text{A6})$$

requiring two long-range fermionic SWAPs per four-qubit block. No additional local SWAPs are necessary.

b. Topology-dependent resource scaling The depth and entangling-gate counts for one four-qubit Givens block under representative connectivity graphs are given in Tab. V. Here d_g denotes the heavy-hex Manhattan distance and ℓ the linear dimension of the square grid. On linear or heavy-hex lattices, the pair-Givens blocks must be executed serially, leading to quadratic depth. Two-dimensional connectivity allows parallel scheduling of non-overlapping blocks, reducing depth to $\mathcal{O}(n)$, while all-to-all connectivity eliminates routing overhead entirely.

c. Single-qubit phase consolidation Many diagonal Z rotations introduced when compiling the phased pair-Givens blocks can be commuted and merged into neighboring blocks (or absorbed into the internal phase parameters of adjacent decompositions), so the *visible* single-qubit *depth* contribution can often be reduced substantially even when the *total* number of single-qubit rotations scales as $\mathcal{O}(n^2)$. The exact consolidation achieved depends on the chosen decomposition of $G_{pq,rs}(\theta, \phi)$ and the scheduling/routing pattern.

4. Preparation versus number-conserving ladder forms

The ladder constructions in Secs. III A and III B admit two closely related realizations, depending on whether the goal is state preparation from the vacuum or basis rotation within an existing many-electron state. Both realizations are generated by the same underlying sequence of Givens rotations and differ only in whether particle injection is included.

a. Preparation form. When the system register is initialized in the vacuum $|0^n\rangle$, the ladder unitaries may be preceded by explicit particle injection using Pauli- X gates on selected pivot orbitals (or pivot pairs),

$$U_{\text{prep}}^{(u)} = U_u X_r \quad \text{or} \quad U_{\text{prep}}^{(u)} = U_u X_r X_s, \quad (\text{A7})$$

for one- and two-electron ladders, respectively. In this form, the circuit prepares the desired few-electron state deterministically from the vacuum and

is useful for initializing reference states or illustrating ladder behavior.

b. Number-conserving form. Omitting the initial particle-injection step yields the strictly number-conserving ladder unitary U_u . This form acts as a basis rotation within a fixed particle-number sector and is agnostic to the specific many-electron state residing on the system register. Crucially, the numerical values of all rotation angles and phases are identical to those used in the preparation form; only the initial excitation is absent.

c. Role in COMPOSER. In the COMPOSER architecture, the number-conserving form U_u is used inside rank-one block-encoding adaptors. This choice ensures that ladder circuits can be applied to arbitrary system states without altering particle number, enabling reuse of a fixed circuit topology across geometry changes, active-space growth, and masked similarity transformations. Particle injection via pivot X gates is therefore a convenience for state preparation, not a requirement for block encoding.

Throughout the remainder of this work, U_u denotes the number-conserving ladder form unless state preparation from the vacuum is stated explicitly.

Appendix B: Proofs and implementation details for rank-one block encodings

This appendix collects proofs and low-level circuit constructions for the rank-one block-encoding primitives introduced in Sec. IV A. The derivations collected are provided for completeness; they do not introduce new primitives beyond standard block-encoding and LCU constructions, but establish correctness and normalization conventions used in the main text. The main text focuses on the resulting adaptor interfaces and how they assemble into a compile-once PREP-SELECT-PREP[†] architecture; the derivations are deferred here for readability.

1. Proof of Lemma 1

Proof. Since \hat{a}_u^\dagger and \hat{a}_v^\dagger are linear combinations of canonical creation operators, applying them to the vacuum produces normalized *one-electron* states (i.e., superpositions of computational-basis determinants with a single occupied orbital):

$$|u\rangle := \hat{a}_u^\dagger |0^n\rangle, \quad |v\rangle := \hat{a}_v^\dagger |0^n\rangle. \quad (\text{B1})$$

Hence the bilinear rank-one operator acts on the *one-electron* sector as

$$\hat{L}_s = \lambda_s \hat{a}_u^\dagger \hat{a}_v = \lambda_s |u\rangle \langle v|. \quad (\text{B2})$$

TABLE V. Depth and entangling-gate counts for one four-qubit Givens block under representative connectivity graphs.

Architecture	Routing cost	CZ gates per block	Depth scaling
Linear / heavy-hex	$(4d_g - 2)$ fSWAPs	$8 + 6(4d_g - 2)$	$\mathcal{O}(n^2)$
2D square grid	$(4\ell - 4)$ fSWAPs	$8 + 6(4\ell - 4)$	$\mathcal{O}(n)$
All-to-all	none	8	$\mathcal{O}(n)$

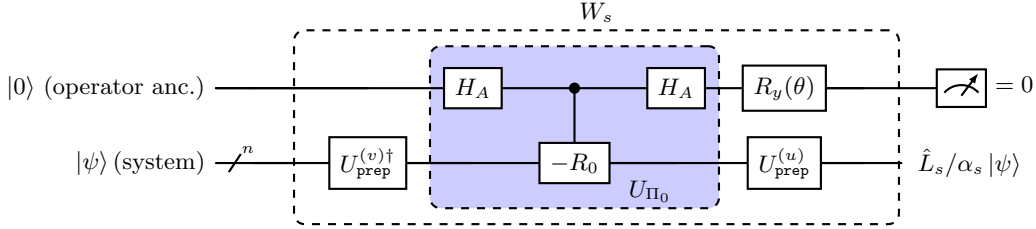


FIG. 9. Sketch of an $(\alpha_s, 1, \epsilon_s)$ block encoding of the dyad $\hat{L}_s = \lambda_s |u\rangle\langle v|$ on the one-excitation subspace, with $\cos(\theta/2) = |\lambda_s|/\alpha_s$ (and an optional phase gate to encode $\arg \lambda_s$ if λ_s is not chosen real). The shaded gadget U_{Π_0} is the standard single-ancilla LCU construction of the vacuum projector $\Pi_0 = |0^n\rangle\langle 0^n|$ from the vacuum reflection $R_0 = I - 2\Pi_0$: $U_{\Pi_0} = (H_A \otimes I)(|0\rangle\langle 0| \otimes I + |1\rangle\langle 1| \otimes (-R_0))(H_A \otimes I)$. Conjugation by $U_{\text{prep}}^{(v)}$ and $U_{\text{prep}}^{(u)}$ yields $(\langle 0| \otimes I) W_s (|0\rangle \otimes I) = |u\rangle\langle v|$.

Let $U_{\text{prep}}^{(u)}$ and $U_{\text{prep}}^{(v)}$ be the deterministic one-electron preparation circuits from Sec. III A satisfying

$$U_{\text{prep}}^{(u)} |0^n\rangle = |u\rangle, \quad U_{\text{prep}}^{(v)} |0^n\rangle = |v\rangle. \quad (\text{B3})$$

Denote by $\Pi_0 := |0^n\rangle\langle 0^n|$ the projector onto the system vacuum.

Introduce a single ancilla qubit A initialized in

$|0\rangle_A$ and define the vacuum reflection

$$R_0 := I_S - 2\Pi_0, \quad \Pi_0 := |0^n\rangle\langle 0^n|. \quad (\text{B4})$$

The unitary R_0 can be implemented as a multi-controlled phase flip on $|0^n\rangle$ (equivalently, conjugating a phase flip on $|1^n\rangle$ by X gates on all system qubits), as indicated schematically in Figure 9.

We first construct a single-ancilla *deterministic* block encoding of Π_0 using a two-branch LCU over $\{I_S, -R_0\}$. Define

$$U_{\Pi_0} := (H_A \otimes I_S) \left(|0\rangle\langle 0|_A \otimes I_S + |1\rangle\langle 1|_A \otimes (-R_0) \right) (H_A \otimes I_S). \quad (\text{B5})$$

A direct calculation gives

$$(\langle 0|_A \otimes I_S) U_{\Pi_0} (|0\rangle_A \otimes I_S) = \frac{1}{2}(I_S - R_0) = \Pi_0, \quad (\text{B6})$$

so U_{Π_0} is a $(1, 1, 0)$ block encoding of Π_0 .

Now define

$$\widetilde{W}_s := (I_A \otimes U_{\text{prep}}^{(u)}) U_{\Pi_0} (I_A \otimes U_{\text{prep}}^{(v)\dagger}). \quad (\text{B7})$$

Projecting the ancilla yields

$$\begin{aligned} (\langle 0|_A \otimes I_S) \widetilde{W}_s (|0\rangle_A \otimes I_S) &= U_{\text{prep}}^{(u)} \Pi_0 U_{\text{prep}}^{(v)\dagger} \\ &= |u\rangle\langle v|. \end{aligned} \quad (\text{B8})$$

Thus \widetilde{W}_s is a $(1, 1, 0)$ block encoding of $|u\rangle\langle v|$.

Finally, since $\hat{L}_s = \lambda_s |u\rangle\langle v|$ has $\|\hat{L}_s\| = |\lambda_s|$, we may choose $\alpha_s := |\lambda_s|$ and (without loss of generality) absorb $\arg(\lambda_s)$ into u or v so that $\lambda_s \in \mathbb{R}_{\geq 0}$. With this choice,

$$(\langle 0|_A \otimes I_S) \widetilde{W}_s (|0\rangle_A \otimes I_S) = \frac{\hat{L}_s}{\alpha_s}. \quad (\text{B9})$$

If a larger normalization $\alpha \geq \alpha_s$ is desired for later multiplexing, it can be handled at the outer LCU layer (i.e., by rescaling coefficients in the selector preparation), without changing the single-ancilla adaptor topology.

The above equalities hold for ideal unitaries. In practice, $U_{\text{prep}}^{(u)}$, $U_{\text{prep}}^{(v)}$, and the multi-controlled im-

plementation of R_0 are synthesized to finite precision, yielding an additive block-encoding error Δ_s with $\|\Delta_s\| \leq \epsilon_s$. \square

2. Proof of Lemma 2

Proof. We work in the rotated basis defined by $U^{(\mu)}$ (applied before the gadget and inverted after). Introduce three ancilla registers: (i) an index register I encoding $\xi \in \{1, \dots, R_\mu\}$, (ii) a flag qubit f , and (iii) a QSVT signal qubit g . All ancillas are initialized in $|0\rangle$.

a. PREP (index loading). Prepare I with amplitudes proportional to $\sqrt{|\lambda_\xi^{(\mu)}|}$:

$$U_{\text{prep}}^{(\mu)} |0\rangle_I = \frac{1}{\sqrt{\Lambda_\mu}} \sum_{\xi=1}^{R_\mu} \sqrt{|\lambda_\xi^{(\mu)}|} |\xi\rangle_I. \quad (\text{B10})$$

This can be synthesized by a unary Givens ladder (depth $\mathcal{O}(R_\mu)$) or a standard binary state-preparation routine (depth $\text{polylog}(R_\mu)$ given classical data access).

b. SELECT (deterministic block encoding of $\hat{n}_{\mu\xi}$). For each ξ , define a two-qubit unitary acting on the rotated system mode ξ and the flag qubit f :

$$W_{\mu\xi} := X_f \text{CNOT}_{\xi \rightarrow f}, \quad (\text{B11})$$

where the control is the system qubit representing occupation of mode ξ in the rotated basis. A direct basis-state check shows that

$$(\langle 0|_f \otimes I) W_{\mu\xi} (|0\rangle_f \otimes I) = \hat{n}_{\mu\xi}. \quad (\text{B12})$$

Thus $W_{\mu\xi}$ is a deterministic $(1, 1, 0)$ block encoding of $\hat{n}_{\mu\xi}$.

Now define the multiplexed SELECT operator

$$U_{\text{sel}}^{(\mu)} = \sum_{\xi=1}^{R_\mu} |\xi\rangle \langle \xi|_I \otimes \left(e^{i\phi_\xi} W_{\mu\xi} \right), \quad (\text{B13})$$

where $\phi_\xi = \arg(\lambda_\xi^{(\mu)})$ (for real eigenvalues, $\phi_\xi \in \{0, \pi\}$), so that $e^{i\phi_\xi} \sqrt{|\lambda_\xi^{(\mu)}|} \sqrt{|\lambda_\xi^{(\mu)}|} = \lambda_\xi^{(\mu)}$.

c. LCU block (encoding \hat{O}_μ). Define the PREP-SELECT-PREP † sandwich

$$U_{\hat{O}_\mu} := U_{\text{prep}}^{(\mu)\dagger} U_{\text{sel}}^{(\mu)} U_{\text{prep}}^{(\mu)}. \quad (\text{B14})$$

Projecting the ancillas (I, f) onto $|0_I 0_f\rangle$ gives

$$\begin{aligned} & (\langle 0|_I \langle 0|_f \otimes I) U_{\hat{O}_\mu} (|0\rangle_I |0\rangle_f \otimes I) \\ &= \frac{1}{\Gamma_\mu} \sum_{\xi=1}^{R_\mu} |\lambda_\xi^{(\mu)}| e^{i\phi_\xi} \hat{n}_{\mu\xi} \\ &= \frac{1}{\Gamma_\mu} \sum_{\xi=1}^{R_\mu} \lambda_\xi^{(\mu)} \hat{n}_{\mu\xi} \\ &= \hat{O}_\mu / \Gamma_\mu, \end{aligned} \quad (\text{B15})$$

which is a deterministic $(\Gamma_\mu, \mathbf{a}_I + 1, 0)$ block encoding of \hat{O}_μ .

d. From \hat{O}_μ to \hat{O}_μ^2 (fixed degree-2 QSVT). Since \hat{O}_μ is Hermitian and $\|\hat{O}_\mu\| \leq \Gamma_\mu$, the above gives a valid block encoding of \hat{O}_μ / Γ_μ . Apply QSVT/QSP with the *exact* polynomial $P_2(x) = x^2$ (degree 2) to this block encoding. That is, there exists a fixed phase list $\varphi^{(2)} = (\varphi_0, \varphi_1, \varphi_2)$ such that the QSVT circuit

$$U_{\hat{O}_\mu^2} := \text{QSVT}(P_2, U_{\hat{O}_\mu}; g) \quad (\text{B16})$$

satisfies

$$\begin{aligned} & (\langle 0|_g \langle 0|_I \langle 0|_f \otimes I) U_{\hat{O}_\mu^2} (|0\rangle_g |0\rangle_I |0\rangle_f \otimes I) \\ &= (\hat{O}_\mu / \Gamma_\mu)^2 = \hat{O}_\mu^2 / \Gamma_\mu^2. \end{aligned} \quad (\text{B17})$$

Because P_2 is implemented exactly, this introduces *no polynomial-approximation error*; the only error source is gate synthesis if angles are approximated.

e. Resources. The PREP stage costs $\mathcal{O}(R_\mu)$ two-qubit gates in a unary ladder and $\text{polylog}(R_\mu)$ depth in standard binary state preparation. The SELECT stage applies a single two-qubit gate $\text{CNOT}_{\xi \rightarrow f}$ (plus X_f) conditioned on ξ ; in unary this is $\mathcal{O}(R_\mu)$ controlled interactions, and in binary it incurs only polylogarithmic decoding overhead on top of $\mathcal{O}(R_\mu)$ controls. The basis rotations $U^{(\mu)}$ and $U^{(\mu)\dagger}$ (if included explicitly) cost $\mathcal{O}(n)$ two-qubit Givens rotations. The degree-2 QSVT step adds a constant overhead: two uses of $U_{\hat{O}_\mu}$ (and/or $U_{\hat{O}_\mu}^\dagger$) and $\mathcal{O}(1)$ single-qubit rotations on the signal qubit g . Ancilla width is \mathbf{a}_I (index) + 1 (flag) + 1 (QSVT signal), with all ancillas initialized and postselected in $|0\rangle$. \square

3. Proof of Theorem 1

Proof. For each s , by hypothesis,

$$(\langle 0^t| \otimes I_S) W_s (|0^t\rangle \otimes I_S) = \hat{L}_s / \alpha_s + \Delta_s, \quad \|\Delta_s\| \leq \epsilon_s.$$

Write $\Omega_s = |\Omega_s| e^{i\phi_s}$ and define the SELECT operator

$$W_{\text{sel}} = \sum_{s=1}^{\ell_H} |s\rangle \langle s| \otimes (e^{i\phi_s} W_s), \quad (\text{B18})$$

which applies $e^{i\phi_s} W_s$ conditioned on the selector state $|s\rangle$. Prepare the selector register using

$$U_{\text{prep}} |0^a\rangle = \frac{1}{\sqrt{\alpha}} \sum_{s=1}^{\ell_H} \sqrt{|\Omega_s| \alpha_s} |s\rangle, \quad \alpha = \sum_{s=1}^{\ell_H} |\Omega_s| \alpha_s. \quad (\text{B19})$$

Define

$$W = (U_{\text{prep}}^\dagger \otimes I) W_{\text{sel}} (U_{\text{prep}} \otimes I).$$

Projecting the $\mathbf{a} + t$ ancillas onto $|0^{a+t}\rangle$ yields

$$\begin{aligned} & \langle\langle 0^{a+t} | \otimes I \rangle\rangle W (|0^{a+t}\rangle \otimes I) \\ &= \frac{1}{\alpha} \sum_s |\Omega_s| \alpha_s \langle\langle 0^t | \otimes I \rangle\rangle e^{i\phi_s} W_s (|0^t\rangle \otimes I) \\ &= \frac{1}{\alpha} \sum_s |\Omega_s| e^{i\phi_s} (\hat{L}_s + \alpha_s \Delta_s) \\ &= \frac{\hat{H}}{\alpha} + \Delta, \end{aligned} \quad (\text{B20})$$

where

$$\Delta = \frac{1}{\alpha} \sum_s |\Omega_s| \alpha_s e^{i\phi_s} \Delta_s, \quad \|\Delta\| \leq \epsilon_{\text{LCU}}.$$

The depth bound follows from the cost of the selector-controlled application of W_s together with the two invocations of the state-preparation unitary U_{prep} . \square

Appendix C: Quantum Signal Processing for Exponentiating Block-Encoded Generators

This appendix summarizes the quantum signal processing (QSP) construction used in Sec. IV B to implement the exponential of a block-encoded anti-Hermitian generator. The material here is standard and included for completeness; see Refs. [50, 51] for full treatments.

1. Polynomial approximation

Let U be a block encoding of a Hermitian operator \hat{A}_s with normalization α , i.e.

$$\langle\langle 0 | \otimes I \rangle\rangle U (|0\rangle \otimes I) = \hat{A}_s / \alpha, \quad \|\hat{A}_s\| \leq \alpha. \quad (\text{C1})$$

To approximate the unitary $e^{-i\hat{A}_s}$, QSP constructs a polynomial $P_d(x)$ such that

$$\sup_{x \in [-1, 1]} |P_d(x) - e^{-i\alpha x}| \leq \epsilon. \quad (\text{C2})$$

A convenient choice is a truncated Chebyshev expansion

$$P_d(x) = \sum_{k=0}^d c_k T_k(x), \quad (\text{C3})$$

where $T_k(x)$ denotes the Chebyshev polynomial of the first kind. For $\alpha > 0$, one may choose an even degree

$$d = \mathcal{O}(\alpha + \log(1/\epsilon)), \quad (\text{C4})$$

which guarantees uniform approximation error ϵ on $[-1, 1]$. This scaling is asymptotically optimal.

2. QSP implementation

Given the polynomial $P_d(x)$, quantum signal processing realizes $P_d(\hat{A}_s/\alpha)$ using a single ancilla qubit and a sequence of phase rotations. Specifically, there exists a phase list $\phi = (\phi_0, \phi_1, \dots, \phi_d)$ such that the unitary

$$Q(\phi, U) = e^{i\phi_0 Z} \prod_{k=1}^d \left(U e^{i\phi_k Z} \right) \quad (\text{C5})$$

satisfies

$$\langle\langle 0 | \otimes I \rangle\rangle Q(\phi, U) (|0\rangle \otimes I) = P_d(\hat{A}_s/\alpha). \quad (\text{C6})$$

The phases $\{\phi_k\}$ depend only on the target function $e^{-i\alpha x}$ and the approximation tolerance ϵ ; they are independent of the internal structure of \hat{A}_s . Consequently, for a *fixed* normalization α the phase list may be computed once classically and reused across different problem instances. If α changes (e.g., under masking), one either recomputes the phase list or fixes a global worst-case normalization and pads the LCU with a null branch so that α remains invariant.

The QSP circuit uses:

- one signal ancilla qubit,
- d controlled applications of the block encoding U ,
- $d + 1$ single-qubit Z rotations.

3. Error propagation

In practice, the block encoding U is approximate:

$$\langle\langle 0 | \otimes I \rangle\rangle U (|0\rangle \otimes I) = \hat{A}_s / \alpha + \Delta, \quad \|\Delta\| \leq \epsilon'. \quad (\text{C7})$$

Applying QSP to such an imperfect block encoding yields

$$\langle\langle 0| \otimes I \rangle\rangle Q(\phi, U) (|0\rangle \otimes I) = e^{-i\hat{A}_s} + \epsilon''(\epsilon', \epsilon), \quad (\text{C8})$$

where the total operator-norm error satisfies

$$\epsilon'' = \mathcal{O}(d\epsilon' + \epsilon). \quad (\text{C9})$$

where the factor of d reflects the d uses of the imperfect block encoding within the QSP sequence (see, e.g., the stability bounds in Refs. [50, 51]). Thus, the overall accuracy is controlled by balancing the block-encoding error ϵ' and the polynomial approximation error ϵ . In Sec. IV B, ϵ' arises from the LCU construction of the generator block encoding, while ϵ is set by the chosen polynomial degree d .

4. Application to the generator $\hat{\sigma}$

In the main text, QSP is applied to the block encoding $U_{\hat{\sigma}}$ of the anti-Hermitian generator $\hat{\sigma} = \sum_s \omega_s \hat{A}_s$ (equivalently, to the Hermitian operator $\hat{A} := i\hat{\sigma}$ via $e^{\hat{\sigma}} = e^{-i\hat{A}}$). Crucially, a *single* QSP ladder suffices to implement $e^{\hat{\sigma}}$, and its degree depends on the chosen normalization (e.g., α' or a fixed global $\bar{\alpha}'$) rather than directly on the number of retained rank-one terms after masking.

Appendix D: Compile–Once Architecture and Error–Depth Tradeoffs

This appendix provides additional detail underlying the compile–once execution model introduced in Sec. V. The material here concerns circuit control overheads, selector–controlled depth scaling, and the relationship between error budgets and overall runtime. These details are not required to understand

the high-level COMPOSER architecture but may be useful for concrete implementations and resource estimation.

1. Selector-controlled adaptor overhead

In the binary-multiplexed constructions of Sec. IV, each rank-one adaptor W_s is executed under control of a selector register. As a result, the relevant depth contribution is that of the *controlled* implementation of W_s , rather than the bare adaptor itself.

For the bilinear rank-one adaptors of Lemma 1, the underlying circuit consists of $\mathcal{O}(n)$ two-qubit Givens rotations acting on the system register and a single signal ancilla. Standard constructions allow each two-qubit gate to be promoted to a selector-controlled version with constant factor overhead, yielding selector-controlled depth $\mathcal{O}(n)$.

For the diagonalized Cholesky-channel adaptors of Lemma 2, the controlled implementation additionally involves index-dependent phase kickback operations. In this case, the selector-controlled depth scales as $\mathcal{O}(n + R_\mu)$, where R_μ is the number of retained rotated modes in channel μ . These overheads are absorbed into the depth estimates used in Sec. IV D.

2. Depth scaling versus error tolerance

The total circuit depth of a similarity-sandwiched oracle $W_{\text{eff}}^{(m)}$ depends parametrically on the total error budget ϵ_{tot} through the quantum signal processing (QSP) degree d as in Eq. (C4). Combining this with the selector-controlled depth of the generator block encoding yields the parametric scaling

$$\text{depth}\left(W_{\text{eff}}^{(m)}\right) = \mathcal{O}\left(\ell_\sigma D_\sigma^{\text{max}} [\bar{\alpha}' + \log(1/\epsilon_{qsp})] + \text{depth}(W_{\text{sel}}(\hat{H}))\right), \quad (\text{D1})$$

up to architecture-dependent constant factors. An explicit mapping from ϵ_{tot} to circuit depth requires specifying a gate-synthesis model that relates ϵ_{block} and ϵ_{mux} to two-qubit gate counts; for this reason, the main text reports parametric rather than hardware-specific expressions.

3. Error-budget allocation

The separation $\epsilon_{\text{tot}} = \epsilon_{\text{factor}} + \epsilon_{\text{block}} + \epsilon_{\text{mux}} + \epsilon_{\text{qsp}}$ introduced in Sec. V permits flexible allocation of error budget across algorithmic layers. While an equal split among contributions provides a convenient baseline, practical implementations may bene-

fit from uneven distributions. For example, on hardware with native arbitrary-angle single-qubit rotations, it may be advantageous to assign a tighter tolerance to ϵ_{block} while allowing a larger ϵ_{qsp} , or vice versa depending on routing constraints and noise characteristics.

The COMPOSER framework does not assume an optimal allocation a priori; rather, it exposes independent control knobs that can be tuned to minimize wall-clock runtime under hardware-specific constraints.

4. Meaning of “compile–once”

As seen in Algorithm 1, “compile–once” in this work denotes invariance of the logical two-qubit circuit topology under instance updates; it does not preclude hardware-level recompilation, pulse recalibration, or changes in fault-tolerant synthesis overhead. Subsequent updates to molecular geometry, active space, or truncation mask modify only single-qubit rotation angles and classical control data, without altering the two-qubit connectivity graph. This distinction is independent of the underlying fault-tolerant or NISQ execution model and should be understood as a circuit-scheduling concept rather than a claim about physical recompilation.

Algorithm 1 COMPOSER: compile stage vs dial stage (“compile–once, dial–later”).

Compile stage (once per orbital pool / qubit mapping):

- 1: Build rank-one ladder pools for \hat{H} and (optionally) $\hat{\sigma}$ via nested factorizations; assign selector addresses.
- 2: Fix ladder pivots and routing schedule; synthesize the adaptor bank, SELECT wiring, and the reusable two-qubit fabric.
- 3: Choose global normalizations $(\alpha, \bar{\alpha}')$ and precompute the QSP phase list ϕ for exponentiating the generator.
- 4: Hardware-map/optimize this two-qubit topology once; store the circuit skeleton with parameter slots.

Dial stage (per geometry / mask / truncation update):

- 5: Recompute classical coefficients $\{\Omega_s\}, \{\omega_s\}$ and choose masks $\mathcal{M}^{(m)}$ (and a model-space projector $P^{(m)}$).
 - 6: Update only single-qubit rotation angles/phases in PREP and local ladder blocks (and, in FT settings, resynthesize rotations to the desired precision).
 - 7: Execute the fixed skeleton to implement $W_{\text{eff}}^{(m)} = U_{\hat{\sigma}}^{(m)\dagger} W U_{\hat{\sigma}}^{(m)}$ and downstream routines.
-

Appendix E: Diagnostics for Fixed Rank–One Algebraic Formulations

This appendix provides supporting analysis for the mask construction and algebraic freezing assumptions used in COMPOSER. The material here is not required for the construction of the block-encoding pipeline, but serves to justify the stability of rank-one operator subspaces and the use of MP2-guided truncation strategies in adaptive similarity transformations.

Within the unitary coupled-cluster doubles (UCCSD) approximation, the anti-Hermitian doubles generator may be written as in Eq. (36),

$$\hat{\sigma}_2 = \sum_s \omega_s (L_s - L_s^\dagger), \quad (\text{E1})$$

where each pair-excitation rank-one operator takes the (antisymmetric) form

$$\hat{L}_s := \hat{B}^\dagger[U^{(s)}] \hat{B}[V^{(s)}], \quad (\text{E2})$$

with $B^\dagger[U^{(s)}]$ and $B[V^{(s)}]$ defined in Eq. (4), and $U^{(s)} \in \wedge^2 \mathbb{C}^{N_v}$ and $V^{(s)} \in \wedge^2 \mathbb{C}^{N_o}$ the antisymmetric pair tensors ($U_{ab}^{(s)} = -U_{ba}^{(s)}$, $V_{ij}^{(s)} = -V_{ji}^{(s)}$). Here $\wedge^2 \mathbb{C}^{N_v}$ denotes the antisymmetric pair space of dimension $\binom{N_v}{2}$. When desired, each antisymmetric tensor may be parameterized by two single-particle vectors via a wedge product, e.g., $U_{ab}^{(s)} = (x_a^{(s)} y_b^{(s)} - x_b^{(s)} y_a^{(s)}) / \sqrt{2}$, and similarly for $V^{(s)}$, matching Sec. II C.

In practical applications, it is desirable to fix the algebraic structure defined by the vectors $\{U^{(s)}, V^{(s)}\}$ and optimize only the scalar coefficients $\{\omega_s\}$. The following sections provide diagnostics and heuristics for assessing when this approximation is justified.

1. Subspace stability diagnostics

A natural diagnostic for algebraic stability is the robustness of the occupied and virtual subspaces under the similarity transformation. We therefore monitor the one-particle reduced density matrices

$$(D^{\text{occ}})_{ij} = \langle \phi_0 | e^{-\hat{\sigma}_2} a_j^\dagger a_i e^{\hat{\sigma}_2} | \phi_0 \rangle, \quad (\text{E3})$$

$$(D^{\text{vir}})_{ab} = \langle \phi_0 | e^{-\hat{\sigma}_2} a_b^\dagger a_a e^{\hat{\sigma}_2} | \phi_0 \rangle, \quad (\text{E4})$$

where $|\phi_0\rangle$ is a reference determinant.

Stability of the algebraic formulation is indicated when the relative change in these density matrices

remains small between successive updates,

$$\frac{\|D^{\text{occ,new}} - D^{\text{occ,ref}}\|_F}{\|D^{\text{occ,ref}}\|_F} \ll 1, \quad (\text{E5})$$

$$\frac{\|D^{\text{vir,new}} - D^{\text{vir,ref}}\|_F}{\|D^{\text{vir,ref}}\|_F} \ll 1, \quad (\text{E6})$$

where $\|\cdot\|_F$ denotes the Frobenius norm. When these conditions are satisfied, the eigenbases defining $\{U^{(s)}, V^{(s)}\}$ remain sufficiently invariant, justifying a fixed algebraic representation. If substantial subspace rotation is detected, the algebraic vectors may be recomputed periodically without altering the overall circuit topology.

2. Subspace-overlap metric for rank-one manifolds (wAUC)

To compare MP2- and CCSD-derived *rank-one* excitation manifolds, we reshape the doubles tensor into a matrix $T \in \mathbb{C}^{N_{Vp} \times N_{Op}}$ with $N_{Vp} = \binom{N_V}{2}$ and $N_{Op} = \binom{N_O}{2}$, indexed by antisymmetric pairs $A \equiv (a < b)$ and $I \equiv (i < j)$. Let the singular value decompositions be $T^{\text{CCSD}} = \sum_k s_k u_k v_k^\dagger$ and $T^{\text{MP2}} = \sum_k \tilde{s}_k \tilde{u}_k \tilde{v}_k^\dagger$. The corresponding rank-one operator basis vectors in the vectorized matrix space are $b_k := \text{vec}(u_k v_k^\dagger) = v_k^* \otimes u_k$ and similarly \tilde{b}_k .

For a chosen rank r , define the orthonormal bases $B_r = [b_1, \dots, b_r]$ and $\tilde{B}_r = [\tilde{b}_1, \dots, \tilde{b}_r]$ and the subspace overlap

$$\text{ov}(r) := \frac{1}{r} \|B_r^\dagger \tilde{B}_r\|_F^2 = \frac{1}{r} \sum_{j=1}^r \cos^2 \theta_j, \quad (\text{E7})$$

where $\{\theta_j\}$ are principal angles between the two r -dimensional subspaces.

We then define a weighted average overlap (wAUC) up to rank R as

$$\text{wAUC}(R) := \sum_{r=1}^R w_r \text{ov}(r) \quad (\text{E8})$$

with $w_r := \frac{s_r^2}{\sum_{k=1}^R s_k^2}$, so that leading singular components contribute most strongly (analogous to explained-variance weighting). In Sec. VII, $R = R_\epsilon$ is determined by the relative screening criterion $s_r/s_1 \geq \epsilon_s$.

3. MP2-guided construction of truncated rank-one operator lists

In weak to moderate correlation regimes, the leading structure of the UCCSD doubles operator is well

captured by second-order Møller–Plesset (MP2) theory. These diagnostics are particularly relevant for Schrieffer–Wolff-style downfolding workflows, where one repeatedly updates generator coefficients (and masks/model spaces) while aiming to preserve a fixed operator manifold and execution topology.

The MP2 doubles amplitudes

$$t_{ab,ij}^{\text{MP2}} = \frac{1}{4} \cdot \frac{\langle ij || ab \rangle}{\epsilon_i + \epsilon_j - \epsilon_a - \epsilon_b} \quad (\text{E9})$$

provide a low-cost proxy for identifying dominant excitation patterns (If one restricts sums to $i < j$ and $a < b$, the factor of 1/4 is omitted; equivalently it may be absorbed into the definition of $t_{ab,ij}^{\text{MP2}}$). Applying the same nested SVD–eigendecomposition used in the main text to $t_{ab,ij}^{\text{MP2}}$ yields an initial rank-one operator list whose algebraic structure is typically stable under subsequent correlation refinement.

a. Ladder weights. As a lightweight ranking heuristic (not a rigorous bound), we assign each rank-one ladder a scalar weight that correlates with its expected contribution to orbital-subspace mixing. A basis-invariant choice consistent with the pair-tensor form in Eq. (E2) is

$$w_s^{\text{MP2}} := |\omega_s|^2 \|U^{(s)}\|_F^2 \|V^{(s)}\|_F^2, \quad (\text{E10})$$

where $\|\cdot\|_F$ denotes the Frobenius norm of the antisymmetric pair tensors (If $U^{(s)}$ and $V^{(s)}$ are normalized by construction, this reduces to $w_s^{\text{MP2}} \propto |\omega_s|^2$). This weight is used only to rank candidate terms and to define cumulative coverage targets in the one-shot mask selection below.

b. One-shot truncation algorithm.

1. **Factorization.** Apply a pivoted approximate SVD to $t_{ab,ij}^{\text{MP2}}$, retaining singular values above a threshold τ_{SVD} , and eigendecompose the resulting vectors with cut-off τ_{ED} to obtain provisional rank-one operators.
2. **Weight evaluation.** Compute w_s^{MP2} for each term and sort the list by decreasing weight.
3. **Mask selection.** Choose the smallest subset S such that the cumulative weight coverage satisfies $\sum_{s \in S} w_s^{\text{MP2}} / \sum_s w_s^{\text{MP2}} \geq \eta$ (e.g., $\eta = 0.99$); the corresponding labels define a selector mask \mathcal{M} .
4. **Optional validation.** After quantum optimization, recompute density matrices with tighter thresholds to verify that subspace deviations remain within tolerance.

In the benchmark set of Sec. VII, retaining only the largest 5–10% of MP2-derived weights typically reproduces both occupied and virtual subspaces to

within 10^{-3} in relative Frobenius norm, while main-

taining a fixed selector width and circuit topology throughout adaptive iterations.

-
- [1] Seth Lloyd. Universal quantum simulators. *Science*, 273(5278):1073–1078, 1996.
- [2] Daniel S. Abrams and Seth Lloyd. Simulation of many-body Fermi systems on a universal quantum computer. *Phys. Rev. Lett.*, 79:2586–2589, 1997.
- [3] Iulia M. Georgescu, Sahel Ashhab, and Franco Nori. Quantum simulation. *Rev. Mod. Phys.*, 86:153–185, 2014.
- [4] Alán Aspuru-Guzik, Anthony D. Dutoi, Peter J. Love, and Martin Head-Gordon. Simulated quantum computation of molecular energies. *Science*, 309(5741):1704–1707, 2005.
- [5] Markus Reiher, Nathan Wiebe, Krysta M. Svore, Dave Wecker, and Matthias Troyer. Elucidating reaction mechanisms on quantum computers. *Proceedings of the National Academy of Sciences*, 114(29):7555–7560, 2017.
- [6] Vera von Burg, Guang Hao Low, Thomas Häner, Damian S. Steiger, Markus Reiher, Martin Roetteler, and Matthias Troyer. Quantum computing enhanced computational catalysis. *Phys. Rev. Res.*, 3:033055, Jul 2021.
- [7] Yudong Cao, Jonathan Romero, Jonathan P. Olson, Matthias Degroote, Peter D. Johnson, Mária Kieferová, Ian D. Kivlichan, Tim Menke, Borja Peropadre, Nicolas P. D. Sawaya, Sukin Sim, Libor Veis, and Alán Aspuru-Guzik. Quantum chemistry in the age of quantum computing. *Chem. Rev.*, 119(19):10856–10915, 2019.
- [8] Sam McArdle, Suguru Endo, Alán Aspuru-Guzik, Simon C. Benjamin, and Xiao Yuan. Quantum computational chemistry. *Rev. Mod. Phys.*, 92:015003, 2020.
- [9] Bela Bauer, Sergey Bravyi, Mario Motta, and Garnet Kin-Lic Chan. Quantum algorithms for quantum chemistry and quantum materials science. *Chemical Reviews*, 120:12685–12717, 2020.
- [10] Jarrod R. McClean, Nicholas C. Rubin, Kevin J. Sung, and Ryan Babbush. OpenFermion: The electronic structure package for quantum computers. *Quantum Sci. Technol.*, 5:034014, 2020.
- [11] Vera von Burg, Martin Roetteler, Gábor Iványos, Ryan Babbush, and Michael E. Beverland. Quantum computing enhanced computational catalysis. *PRX Quantum*, 2:030305, 2022.
- [12] Ivan Kassal, James D. Whitfield, Alejandro Perdomo-Ortiz, Man-Hong Yung, and Alán Aspuru-Guzik. Polynomial-time quantum algorithm for the simulation of chemical dynamics. *Proc. Natl. Acad. Sci. U. S. A.*, 105(48):18681–18686, 2008.
- [13] James D. Whitfield, Jacob Biamonte, and Alán Aspuru-Guzik. Simulation of electronic structure hamiltonians using quantum computers. *Mol. Phys.*, 109(5):735–750, 2011.
- [14] Alan Bidart, Prateek Vaish, Tilas Kabengele, Yaoqi Pang, Yuan Liu, and Brenda M. Rubenstein. Quantum computing beyond ground state electronic structure: A review of progress toward quantum chemistry out of the ground state. *Preprint*, page arXiv:2509.19709, 2025.
- [15] Jules Tilly, Hongxiang Chen, Shuxiang Cao, and et al. The variational quantum eigensolver: A review of methods and best practices. *Phys. Rep.*, 986:1–128, 2022.
- [16] Dominic W. Berry, Kianna Wan, Andrew D. Baczewski, Elliot C. Eklund, Arkin Tikku, and Ryan Babbush. Quantum simulation of chemistry via quantum fast multipole method. *Preprint*, page arXiv:2510.07380, 2025.
- [17] Felipe H. da Jornada, Matteo Lostaglio, et al. A comprehensive framework to simulate real-time chemical dynamics on a fault-tolerant quantum computer. *Preprint*, page arXiv:2504.06348, 2025.
- [18] Mario Motta, Jinzhao Sun, Austin T. K. Tan, et al. Determining ground-state energies using quantum imaginary time evolution. *Nat. Phys.*, 16:205–210, 2020.
- [19] Kazuhiro Seki and Seiji Yunoki. Quantum power method by a superposition of time-evolved states. *PRX Quantum*, 2:010333, Feb 2021.
- [20] John Preskill. Quantum computing in the NISQ era and beyond. *Quantum*, 2:79, 2018.
- [21] Dave Wecker, Matthew B. Hastings, and Matthias Troyer. Progress towards practical quantum variational algorithms. *Phys. Rev. A*, 92:042303, 2015.
- [22] Abhinav Kandala, Antonio Mezzacapo, Kristan Temme, Maika Takita, Markus Brink, Jerry M. Chow, and Jay M. Gambetta. Hardware-efficient variational quantum eigensolver for small molecules and quantum magnets. *Nature*, 549:242–246, 2017.
- [23] Kishor Bharti, Alba Cervera-Lierta, Thi Ha Kyaw, Tobias Haug, Sumner Alperin-Lea, Abhinav Anand, Matthias Degroote, Hermanni Heimonen, Jakob S. Kottmann, Tim Menke, Wai-Keong Mok, Sukin Sim, Leong-Chuan Kwek, and Alán Aspuru-Guzik. Noisy intermediate-scale quantum algorithms. *Rev. Mod. Phys.*, 94:015004, Feb 2022.
- [24] M. Cerezo, A. Arrasmith, R. Babbush, et al. Variational quantum algorithms. *Nat. Rev. Phys.*, 3:625–644, 2021.
- [25] Suguru Endo, Zhenyu Cai, Simon C. Benjamin, and Xiao Yuan. Hybrid quantum-classical algorithms and quantum error mitigation. *J. Phys. Soc. Japan*, 90:032001, 2021.
- [26] Kenji Sugisaki, Seisuke Kanno, Toshiki Itoko, Rito Sakuma, and Naoki Yamamoto. Quantum simulation of chemistry in the fault-tolerant era. *Phys. Chem. Chem. Phys.*, 27:20869–20884, 2025.

- [27] Yukun Zhang, Xiaoming Zhang, Jinzhao Sun, Heng Lin, Yifei Huang, Dingshun Lv, and Xiao Yuan. Quantum algorithms for quantum molecular systems: A survey. *WIREs Comput. Mol. Sci.*, 15(3):e70020, 2025.
- [28] Jarrod R. McClean, Melisa E. Kimchi-Schwartz, Jonathan Carter, and Wibe A. de Jong. Hybrid quantum-classical hierarchy for mitigation of decoherence and determination of excited states. *Phys. Rev. A*, 95:042308, 2017.
- [29] William J. Huggins, Joonho Lee, Unpil Baek, Bryan O’Gorman, and K. Birgitta Whaley. A non-orthogonal variational quantum eigensolver. *New J. Phys.*, 22:073009, 2020.
- [30] Unpil Baek, Diptarka Hait, James Shee, Oskar Leimkuhler, William J. Huggins, Torin F. Stetina, Martin Head-Gordon, and K. Birgitta Whaley. Say no to optimization: A nonorthogonal quantum eigensolver. *PRX Quantum*, 4:030307, 2023.
- [31] Muqing Zheng, Bo Peng, Nathan Wiebe, Ang Li, Xiu Yang, and Karol Kowalski. Quantum algorithms for generator coordinate methods. *Phys. Rev. Research*, 5:023200, 2023.
- [32] Muqing Zheng, Bo Peng, Ang Li, Xiu Yang, and Karol Kowalski. Unleashed from constrained optimization: quantum computing for quantum chemistry employing generator coordinate inspired method. *npj Quantum Inf.*, 10:127, 2024.
- [33] J. R. Schrieffer and P. A. Wolff. Relation between the Anderson and Kondo hamiltonians. *Phys. Rev.*, 149:491–492, 1966.
- [34] Sergey Bravyi, David P. DiVincenzo, and Daniel Loss. Schrieffer–wolf transformation for quantum many-body systems. *Ann. Phys.*, 326(10):2793–2826, 2011.
- [35] Susumu Okubo. Diagonalization of hamiltonian and tamm-dancoff equation. *Prog. Theor. Phys.*, 12(5):603–622, 1954.
- [36] Claude Bloch and Jules Horowitz. Sur la détermination des premiers états d’un système de fermions dans le cas dégénéré. *Nucl. Phys.*, 8:91–105, 1958.
- [37] Herman Feshbach. Unified theory of nuclear reactions. *Ann. Phys.*, 5:357–390, 1958.
- [38] Takeshi Yanai and Garnet Kin-Lic Chan. Canonical transformation theory for dynamic correlation in multireference problems. *J. Chem. Phys.*, 127:104107, 2007.
- [39] Gerald Knizia and Garnet Kin-Lic Chan. Density matrix embedding: A simple alternative to dynamical mean-field theory. *Phys. Rev. Lett.*, 109:186404, 2012.
- [40] Antoine Georges, Gabriel Kotliar, Werner Krauth, and Marcelo J. Rozenberg. Dynamical mean-field theory of strongly correlated fermion systems and the limit of infinite dimensions. *Rev. Mod. Phys.*, 68:13–125, 1996.
- [41] Tomasz A. Wesolowski and Arieh Warshel. Frozen density functional approach for ab initio calculations of solvated molecules. *J. Phys. Chem.*, 97:8050–8053, 1993.
- [42] Christoph R. Jacob and Johannes Neugebauer. Subsystem density-functional theory (update). *WIREs Comput. Mol. Sci.*, 14(1):e1700, 2024.
- [43] Franz Wegner. Flow-equations for hamiltonians. *Ann. Phys.*, 506(2):77–91, 1994.
- [44] Stanislaw D. Glazek and Kenneth G. Wilson. Renormalization of hamiltonians. *Phys. Rev. D*, 48(12):5863–5872, 1993.
- [45] Stefan Kehrein. *The Flow Equation Approach to Many-Particle Systems*, volume 217 of *Springer Tracts in Modern Physics*. Springer, 2006.
- [46] Rolando D. Somma, Gerardo Ortiz, Emanuel Knill, and James E. Gubernatis. Simulating physical phenomena by quantum networks. *Phys. Rev. A*, 65:042323, 2002.
- [47] Daniel S. Abrams and Seth Lloyd. Quantum algorithm providing exponential speed increase for finding eigenvalues and eigenvectors. *Phys. Rev. Lett.*, 83:5162–5165, 1999.
- [48] Andrew M. Childs and Nathan Wiebe. Hamiltonian simulation using linear combinations of unitary operations. *Quantum Info. Comput.*, 12(11–12):901–924, 2012.
- [49] Dominic W. Berry, Andrew M. Childs, and Robin Kothari. Hamiltonian simulation with nearly optimal dependence on all parameters. *Proceedings of the 56th Annual IEEE Symposium on Foundations of Computer Science (FOCS)*, pages 792–809, 2015.
- [50] Guang Hao Low and Isaac L. Chuang. Optimal hamiltonian simulation by quantum signal processing. *Phys. Rev. Lett.*, 118:010501, 2017.
- [51] András Gilyén, Yuan Su, Guang Hao Low, and Nathan Wiebe. Quantum singular value transformation and beyond: Exponential improvements for quantum matrix arithmetics. In *Proceedings of the 51st Annual ACM SIGACT Symposium on Theory of Computing (STOC)*, pages 193–204, 2019.
- [52] Guang Hao Low and Isaac L. Chuang. Hamiltonian simulation by qubitization. *Quantum*, 3:163, 2019.
- [53] Andrew M. Childs, Dmitri Maslov, Yunseong Nam, Neil J. Ross, and Yuan Su. Toward the first quantum simulation with quantum speedup. *Proc. Natl. Acad. Sci. U. S. A.*, 115(38):9456–9461, 2018.
- [54] Andrew M. Childs, Yuan Su, Minh C. Tran, Nathan Wiebe, and Shuchen Zhu. Theory of trotter error with commutator scaling. *Phys. Rev. X*, 11:011020, 2021.
- [55] Guang Hao Low, Nathan Wiebe, Dominic W. Berry, et al. Fast quantum simulation of electronic structure in chemistry by spectrum amplification. *Phys. Rev. X*, 15:041016, 2025.
- [56] Dario Rocca, Maximilian West, Taisei Zexler, and Ryan Babbush. Qubitization of doubly factorized hamiltonians with stochastic-cddf. *J. Chem. Theory Comput.*, 20(11):4639–4653, 2024.
- [57] Diyi Liu, Daochen Zhu, Guang Hao Low, Lin Lin, and Yu Yang. Block encoding with low gate count for second-quantized hamiltonians. *Preprint*, page arXiv:2510.08644, 2025.
- [58] Diyi Liu, Weijie Du, Lin Lin, James P. Vary, and

- Chao Yang. An efficient quantum circuit for block encoding a pairing hamiltonian. *J. Comput. Sci.*, 85:102480, 2025.
- [59] J. L. Whitten. Coulombic potential energy integrals and approximations. *J. Chem. Phys.*, 58(10):4496–4501, 05 1973.
- [60] O. Vahtras, J. Almlöf, and M.W. Feyereisen. Integral approximations for lcao-scf calculations. *Chem. Phys. Lett.*, 213(5):514–518, 1993.
- [61] Nelson H. F. Beebe and Jørgen Linderberg. Simplifications in the generation and transformation of two-electron integrals in molecular calculations. *Int. J. Quantum Chem.*, 12(4):683–705, 1977.
- [62] Francesco Aquilante, Thomas B. Pedersen, and Roland Lindh. Cholesky decomposition of the two-electron integral matrix in electronic structure theory. *J. Chem. Phys.*, 126:194106, 2007.
- [63] Ivar Røeggen and Tor S. Johansen. Cholesky decomposition of the two-electron integral matrix in electronic structure theory. *J. Chem. Phys.*, 128:194107, 2008.
- [64] Thomas Bondo Pedersen, Susi Lehtola, Ignacio Fdez. Galván, and Roland Lindh. The versatility of the cholesky decomposition in electronic structure theory. *WIREs Comput. Mol. Sci.*, 14(1):e1692, 2024.
- [65] Edward G. Hohenstein, Robert M. Parrish, and Todd J. Martínez. Tensor hypercontraction of the electron repulsion integrals. i. theoretical aspects. *J. Chem. Phys.*, 137:044103, 2012.
- [66] Robert M. Parrish, Edward G. Hohenstein, Todd J. Martínez, and C. David Sherrill. Tensor hypercontraction. ii. least-squares renormalization. *J. Chem. Phys.*, 137(22):224106, 12 2012.
- [67] Bo Peng and Karol Kowalski. Highly efficient and scalable compound decomposition of two-electron integral tensor and its application in coupled cluster calculations. *J. Chem. Theory Comput.*, 13(9):4179–4192, 2017.
- [68] Dominic W. Berry, Craig Gidney, Mario Motta, Jarrod R. McClean, and Ryan Babbush. Qubitization of arbitrary basis quantum chemistry leveraging sparsity and low rank factorization. *Quantum*, 3:208, 2019.
- [69] Mario Motta, Erika Ye, Jarrod R. McClean, Zhen-dong Li, Austin J. Minnich, Ryan Babbush, and Garnet Kin-Lic Chan. Low rank representations for quantum simulation of electronic structure. *npj Quantum Inf.*, 7:83, 2021.
- [70] Ian D. Kivlichan, Jarrod McClean, Nathan Wiebe, Craig Gidney, Alán Aspuru-Guzik, Garnet Kin-Lic Chan, and Ryan Babbush. Quantum simulation of electronic structure with linear depth and connectivity. *Phys. Rev. Lett.*, 120:110501, 2018.
- [71] Ryan Babbush, Dominic W. Berry, Ian D. Kivlichan, Nathan Wiebe, Craig Gidney, Alán Aspuru-Guzik, and Garnet Kin-Lic Chan. Low-depth quantum simulation of materials. *Phys. Rev. X*, 8:011044, 2018.
- [72] Ryan Babbush, Craig Gidney, Dominic W. Berry, Nathan Wiebe, Jarrod McClean, Alexandru Paler, Austin Fowler, and Hartmut Neven. Encoding electronic spectra in quantum circuits with linear t complexity. *Phys. Rev. X*, 8:041015, Oct 2018.
- [73] Robert M. Parrish, Edward G. Hohenstein, and Todd J. Martínez. Rank-reduced coupled cluster theory. i. ground state energies and wavefunctions. *J. Chem. Phys.*, 150:164118, 2019.
- [74] Edward G. Hohenstein, Janus J. Eriksen, Andreas J. Thorvaldsen, Shirin Faraji, and Poul Jørgensen. Rank-reduced coupled cluster theory. iii. compressed representations of the coupled cluster doubles amplitudes. *J. Chem. Phys.*, 157:054103, 2022.
- [75] Alberto Peruzzo, Jarrod McClean, Peter Shadbolt, Man-Hong Yung, Xiao-Qi Zhou, Peter J. Love, Alán Aspuru-Guzik, and Jeremy L. O’Brien. A variational eigenvalue solver on a photonic quantum processor. *Nat. Commun.*, 5:4213, 2014.
- [76] Jarrod R. McClean, Jonathan Romero, Ryan Babbush, and Alán Aspuru-Guzik. The theory of variational hybrid quantum-classical algorithms. *New J. Phys.*, 18:023023, 2016.
- [77] Peter J. J. O’Malley, Ryan Babbush, Ian D. Kivlichan, et al. Scalable quantum simulation of molecular energies. *Phys. Rev. X*, 6:031007, 2016.
- [78] Chr. Møller and M. S. Plesset. Note on an approximation treatment for many-electron systems. *Phys. Rev.*, 46(7):618–622, 1934.
- [79] Trygve Helgaker, Poul Jørgensen, and Jeppe Olsen. *Molecular Electronic-Structure Theory*. Wiley, 2000.
- [80] Y. Nam, J.S. Chen, and N.C. et al. Pisenti. Ground-state energy estimation of the water molecule on a trapped-ion quantum computer. *npj Quantum Inf.*, 6:33, 2020.
- [81] Alexander Cowtan, Silas Dilkes, Ross Duncan, Alexandre Krajenbrink, Will Simmons, and Seyon Sivarajah. On the Qubit Routing Problem. In Wim van Dam and Laura Mančinska, editors, *14th Conference on the Theory of Quantum Computation, Communication and Cryptography (TQC 2019)*, volume 135 of *Leibniz International Proceedings in Informatics (LIPIcs)*, pages 5:1–5:32, Dagstuhl, Germany, 2019. Schloss Dagstuhl – Leibniz-Zentrum für Informatik.
- [82] Seyon Sivarajah, Silas Dilkes, Alexander Cowtan, Will Simmons, Alec Edgington, and Ross Duncan. t|ket>: A retargetable compiler for NISQ devices. *Quantum Sci. Technol.*, 6:014003, 2020.
- [83] Alwin Zulehner, Alexandru Paler, and Robert Wille. An efficient methodology for mapping quantum circuits to the IBM QX architectures. In *Proceedings of the Design Automation Conference (DAC)*, 2018.
- [84] Harper R. Grimsley, Sophia E. Economou, Edwin Barnes, and Nicholas J. Mayhall. An adaptive variational algorithm for exact molecular simulations on a quantum computer. *Nat. Commun.*, 10:3007, 2019.
- [85] Dominic W. Berry, Craig Gidney, Mario Motta, Jarrod R. McClean, and Ryan Babbush. Improved

- techniques for preparing eigenstates of fermionic hamiltonians. *npj Quantum Information*, 4:22, 2018.
- [86] Prithvi Gundlapalli and Junyi Lee. Deterministic and entanglement-efficient preparation of amplitude-encoded quantum registers. *Phys. Rev. Appl.*, 18:024013, Aug 2022.
- [87] Daniel K. Park, Francesco Petruccione, and June-Koo Kevin Rhee. Circuit-based quantum random access memory for classical data. *Sci. Rep.*, 9:3949, 2019.
- [88] David Motlagh, Nathan Wiebe, and Dominic W. Berry. Generalized quantum signal processing. *PRX Quantum*, 5:020368, 2024.
- [89] Dominic W. Berry, Danial Motlagh, Giacomo Pantaleoni, and Nathan Wiebe. Doubling the efficiency of hamiltonian simulation via generalized quantum signal processing. *Phys. Rev. A*, 110:012612, Jul 2024.
- [90] N. N. Bogoljubov. On a new method in the theory of superconductivity. *Nuovo Cim.*, 7(6):794–805, 1958.
- [91] J. G. Valatin. Comments on the theory of superconductivity. *Nuovo Cim.*, 7(6):843–857, 1958.
- [92] Robert Jastrow. Many-body problem with strong forces. *Phys. Rev.*, 98:1479–1484, 1955.
- [93] Brett I. Dunlap. Robust and variational fitting. *Phys. Chem. Chem. Phys.*, 2:2113–2116, 2000.
- [94] Vadym Kliuchnikov, Dmitri Maslov, and Michele Mosca. Asymptotically optimal approximation of single qubit unitaries by clifford and T circuits. *Phys. Rev. Lett.*, 110:190502, 2013.
- [95] Peter Selinger. Efficient clifford+t approximation of single-qubit operators. *Quantum Info. Comput.*, 15(1–2):159–180, January 2015.
- [96] Matthew Amy, Dmitri Maslov, Michele Mosca, and Martin Roetteler. A meet-in-the-middle algorithm for fast synthesis of depth-optimal quantum circuits. *IEEE TCAD*, 32(6):818–830, 2013.
- [97] Mario Motta, Kevin J. Sung, K. Birgitta Whaley, Martin Head-Gordon, and James Shee. Bridging physical intuition and hardware efficiency for correlated electronic states: the local unitary cluster jastrow ansatz for electronic structure. *Chem. Sci.*, 14(40):11213–11227, 2023.
- [98] Yuta Matsuzawa and Yuki Kurashige. Jastrow-type decomposition in quantum chemistry for low-depth quantum circuits. *J. Chem. Theory Comput.*, 16:944–952, 2020.
- [99] John P. T. Stenger, C. Stephen Hellberg, and Daniel Gunlycke. Implementing jastrow–gutzwiller operators on a quantum computer using the cascaded variational quantum eigensolver algorithm. *Phys. Rev. A*, 107(6):062606, 2023.
- [100] F. Verstraete, V. Murg, and J.I. Cirac. Matrix product states, projected entangled pair states, and variational renormalization group methods for quantum spin systems. *Adv. Phys.*, 57(2):143–224, 2008.
- [101] Román Orús. A practical introduction to tensor networks: Matrix product states and projected entangled pair states. *Ann. Phys.*, 349:117–158, 2014.
- [102] Gregory M. Crosswhite and Dave Bacon. Finite automata for caching in matrix product algorithms. *Phys. Rev. A*, 78:012356, 2008.
- [103] Steven R. White. Density matrix formulation for quantum renormalization groups. *Phys. Rev. Lett.*, 69:2863–2866, 1992.
- [104] Ulrich Schollwöck. The density-matrix renormalization group in the age of matrix product states. *Ann. Phys.*, 326:96–192, 2011.
- [105] Garnet Kin-Lic Chan and Sandeep Sharma. The density matrix renormalization group in quantum chemistry. *Ann. Rev. Phys. Chem.*, 62:465–481, 2011.
- [106] Sebastian Keller, Michele Dolfi, Matthias Troyer, and Markus Reiher. An efficient matrix product operator representation of the quantum chemical hamiltonian. *J. Chem. Phys.*, 143(24):244118, 2015.